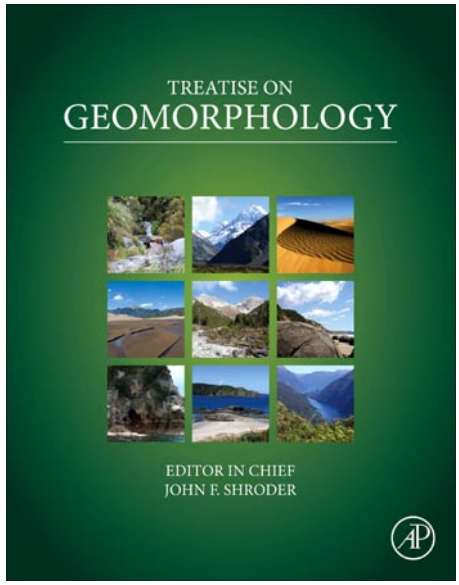

Mitasova H., Barton M., Ullah I., Hofierka J., and Harmon R.S. (2013) GIS-Based Soil Erosion Modeling. In: John F. Shroder (ed.) Treatise on Geomorphology, Volume 3, pp. 228-258. San Diego: Academic Press.

3.9 GIS-Based Soil Erosion Modeling

H Mitasova, North Carolina State University, Raleigh, NC, USA
M Barton and I Ullah, Arizona State University, Tempe, AZ, USA
J Hofierka, Pavol Jozef Safarik University, Kosice, Slovakia
RS Harmon, North Carolina State University, Raleigh, NC, USA

Symbols

(x, y) (m)	georeferenced coordinates
t (s)	time
$\rho_s(x, y, t)$ (kg m^{-3})	sediment mass density
$h(x, y, t)$ (m)	water flow depth
$\mathbf{q}_s(x, y, t)$ (kg (ms)$^{-1}$)	direction and rate of sediment flow per unit width
$q_s = \lvert\mathbf{q}_s\rvert$	magnitude of sediment flow rate per unit width
∇	divergence of a flow vector field
$d_s(x, y, t)$ (kg m^{-2}s^{-1})	net erosion or deposition rate
$\mathbf{q}(x, y, t)$ (m^2 s^{-1})	direction and rate of water flow per unit width
T_c (kg (ms)$^{-1}$)	sediment transport capacity
D_c (kg m^{-2} s^{-1})	detachment capacity
σ (m^{-1})	first-order reaction term dependent on land cover properties
K_t(s)	effective sediment transport capacity coefficient
K_d (s m^{-1})	effective erodibility (detachment capacity coefficient)
τ(Pa=kg m^{-2})	shear stress
τ_0 (Pa)	critical shear stress
a, b, m, n	empirical exponents
β (deg)	surface slope angle
$S = \tan\beta$	surface slope (rise over run)
$g_w = \rho_w g$	hydrostatic pressure of water with the unit height
$g = 9.81$ (m s^{-2})	gravitational acceleration

Mitasova, H., Barton, M., Ullah, I., Hofierka, J., Harmon, R.S., 2013. GIS-based soil erosion modeling. In: Shroder, J. (Editor in Chief), Bishop, M.P. (Ed.), Treatise on Geomorphology. Academic Press, San Diego, CA, vol. 3, Remote Sensing and GIScience in Geomorphology, pp. 228–258

$\rho_w = 10^3$ (kg m^{-3})	mass density of water
v (m s^{-1})	stream velocity
n	Manning's coefficient
ω (J (ms)$^{-1}$)	the unit stream power
D (kg m^{-2} yr^{-1})	average annual soil loss
R (M J mm (ha hr yr)$^{-1}$)	rainfall factor
K (ton ha hr (ha M J mm)$^{-1}$)	soil erodibility factor
LS	dimensionless topographic (length-slope) factor
L (m)	hillslope length
$L_0 = 22.23$ m	length of the standard USLE experimental plot
C	dimensionless land-cover factor
P	dimensionless prevention measures factor
U (m^2 m^{-1})	upslope contributing area per unit width
A (m^2)	upslope contributing area
$\mathbf{s}_0 = (\cos\alpha, \sin\alpha)$	unit vector in the steepest slope direction
α (deg)	aspect angle equivalent to the direction of flow
κ_p (m^{-1})	profile curvature (normal curvature in gradient direction, rate of change in slope)
κ_t (m^{-1})	tangential curvature (normal curvature in the direction perpendicular to the gradient, rate of change in aspect)
κ_h (m^{-1})	plan curvature (tangential curvature projected to horizontal plane)
P_e	channel erosion index
w	topographic wetness index
z (m)	elevation
γ (m^2 s^{-1})	sediment transport diffusion constant
K_g (m(1000 yr)$^{-1}$)	long term diffusion coefficient
r (m)	rainfall excess

Glossary

Detachment capacity Maximum potential soil detachment by overland flow.

Erosion by overland flow Detachment of soil particles by raindrop impact and their removal downslope by water flowing overland as a sheet or in small concentrated flow channels called rills.

Gully erosion Detachment of soil by surface water flow concentrated in rapidly developing channel via headwall or knickpoint migration.

Landscape evolution The change in the altitude and morphology of the topography over time given variations in erosion and deposition caused by numerous surface processes.

Net erosion and deposition Soil mass that is lost or gained at a unit area for a unit time due to removal, transport, or deposition by water flow.

Rill erosion Removal of soil particles by water flowing in small concentrated flow channels called rills.

Sediment transport capacity Maximum potential sediment transport by overland flow.

Shear stress Force of moving water against the bed of the channel.

Stream power Rate of energy dissipation against the bed and banks of a stream per unit downstream length.

Topographic erosion factor Measure of terrain impact on erosion rates, computed as a function of water flow proxy (hillslope length or contributing area) and slope angle.

Universal Soil Loss Equation Simple empirical equation for estimation of annual soil loss rate for hillslopes with simple geometry.

Water Erosion Prediction Project Process-based continuous time modeling system for prediction of sediment yield and erosion/deposition in small watersheds.

Abstract

This chapter explains the theory and methods for GIS-based modeling of soil erosion, sediment transport, and deposition by surface water flow. The mathematical foundations of erosion models are introduced and simplified equations, suitable for GIS implementation, are derived. The presented methods cover modeling of hillslope erosion and deposition, gully formation, and landscape evolution processes. Coupling of erosion models with GIS is discussed, followed by examples of GIS implementation of simple and advanced models. The concepts and methods are illustrated using two case studies, that focus on feedbacks between the human activity and landscape processes.

3.9.1 Introduction

The Earth's surface, exposed to gravitational forces, wind, water, and ice action, continuously evolves over wide range of spatial and temporal scales. Erosion processes that form the land surface are extremely complex, poorly understood, and hard to predict quantitatively over large landscapes (Finlayson and Montgomery, 2003). Remote sensing provides important

data that allow us to gain insights into interactions between physical processes and environmental conditions that control erosion and landform evolution. Recent advances in mapping technologies, such as Light Detection and Ranging (LiDAR), hyperspectral imaging, and ground penetrating radar have dramatically increased the spatial and temporal resolution of Earth surface and shallow subsurface monitoring. The new, more detailed data indicate that fundamental changes in the underlaying theory of erosion processes may be needed to align it with the new observations. Geospatial information science (GISc)-based analysis and modeling plays an important role in integrating observations and models, and improves understanding and prediction capabilities aimed at minimizing negative impacts of erosion and sedimentation.

3.9.2 Background

3.9.2.1 Erosion Processes

Erosion encompasses a broad range of processes that involve soil detachment and transport due to forces that act upon Earth surface. Remote sensing and field-based geospatial technology provides effective tools for detecting and mapping specific landforms that are created by different driving forces, including (**Figure 1**):

- soil erosion by overland flow (sheet, rill, gully),
- channel erosion by fluvial processes,
- gravitational erosion, landslides, debris flow,
- wind erosion,
- coastal erosion by surge and waves,
- glacial erosion.

Fundamentals of erosion processes and quantitative modeling are covered in the relevant volumes of this series. Although all types of erosion have been, at least to some extent, analyzed or modeled using remote sensing data and geographic information system (GIS) tools, most focus has been on soil erosion by overland flow, due to its impact on agricultural productivity, water quality, and sustainable land management. Therefore, in this chapter, the emphasis is on erosion, sediment transport, and deposition driven by surface water flow.

3.9.2.2 Spatial Variability

GIS-based modeling of soil erosion investigates spatial patterns of soil detachment, transport and deposition, and their impact on landscape evolution. Several approaches are used to develop models of erosion processes: 'Empirical or statistical models' derive the governing equations from monitoring data or field experiments using statistical methods such as regression. 'Rule-based models' are constructed from general observations that relate a combination of inputs to observed result, implemented as logical operations such as overlays. 'Physics-based models' use equations derived from natural laws, such as continuity of mass and energy conservation. Specific model implementations commonly combine approaches, for example, physics-based, sediment transport routing with empirically derived parameters (Renschler, 2003; Mitasova et al., 2005b). Spatial variability in landscape-scale, soil-erosion processes requires discretization of landscape representation in GIS-based models.

Spatially averaged hydrologic units are commonly employed in rule-based models (indexes and conditional overlays) or spatially averaged, process-based models. For example, when modeling erosion by surface water flow, units with simple geometry (tilted planes or polylines) represent hillslope segments, watershed hierarchies, channels, and stream networks (**Figure 2**). The processes are then described by unit-to-unit transport rules or by ordinary differential equations for quasiunivariate transport. This approach is very effective for systems that include anthropogenic features (ditches, sediment control structures), but selection of suitable spatial units, their network topology and hierarchies require substantial expertise and can significantly influence the results (Arabi et al., 2006). This is true especially for complex, natural environments that cannot be easily described by simple geometrical features and where spatially averaged models have limited capabilities to identify precise location of sediment sources and sinks, and the pattern of their propagation through landscapes. By reducing the size of the discrete units, especially in locations with complex topography, spatial pattern of erosion can be captured at the level of detail that approaches the fully distributed models. For example, the combined Water Erosion Prediction Project (WEPP) and GeoWEPP model supports modeling at three different levels of spatial detail – watershed, user-defined hillslope segments, and flow-paths (Renschler, 2003).

Spatially distributed models represent the input variables and modeled values as continuous fields, usually discretized as regular grids or irregular meshes. As opposed to the spatially averaged models that predict erosion rates for an area of a discrete spatial unit, the distributed models predict the modeled values for any point in space and provide detailed spatial patterns of sediment sources and sinks (**Figure 2**). On the other hand, these models are complex in terms of data inputs and calibration, and the quantitative summary predictions (e.g., total sediment loads at a watershed outlet) are not necessarily more accurate than the predictions by simpler, spatially averaged models.

Erosion and sediment transport is a multiscale process and different processes require modeling at different spatial resolutions. At hillslope scale, sheet and rill erosion dominate and their accurate spatial modeling requires submeter resolution. Watershed scale uses averaged sheet and rill erosion representation and generally captures large gullies and channels. Depending on the size of the modeled watershed and its channels, 1–10 m resolution is required. Regional scale modeling of large watersheds (thousands of square km), averages sheet, rill and gully erosion, and uses simplified channel representations and spatially averaged hydrologic units. The resolutions of input data and results range from 30 m to hundreds of meters. Irregular meshes and hydrologic units provide means to adjust the level of detail to the complexity of landscape features and support spatially variable scale.

3.9.2.3 Temporal Variability

Simple empirical erosion models assume relatively steady erosion over time and estimate long-term, average annual

Figure 1 Erosion caused by surface water flow: (a) rills, (b) gullies, (c) stream bank erosion.

erosion rates based on empirical factors derived from long-term observations. In reality, erosion rates change rapidly due to the highly dynamic nature of the driving forces, such as rainfall and water flow, over multiple temporal scales. The full dynamics of erosion processes are difficult to capture due to complex, multiscale interactions and limited temporal resolution of the input data. Therefore, modeling is commonly performed for the steady state case associated with peak flows during individual erosion events. Sophisticated modeling systems then perform continuous time simulations of several interacting processes that incorporate steady-state impacts of rainfall events over several years. For example, the WEPP model simulates daily changes in soil and vegetation (crops) and when rainfall occurs, the plant and soil characteristics are used to determine whether surface runoff will occur or not. If runoff is predicted, sheet, rill, and channel sediment detachment and deposition are computed. The model thus simulates impacts of climate (rainfall, temperature, solar radiation), hydrology (infiltration, depressional storage and runoff), water balance (evapotranspiration, percolation, and drainage), vegetation growth (cropland, rangeland, and forest), erosion (interrill, rill, channel), and deposition (in rills, channels, and impoundments). In addition to continuous time simulations, WEPP can be used to assess impact of a

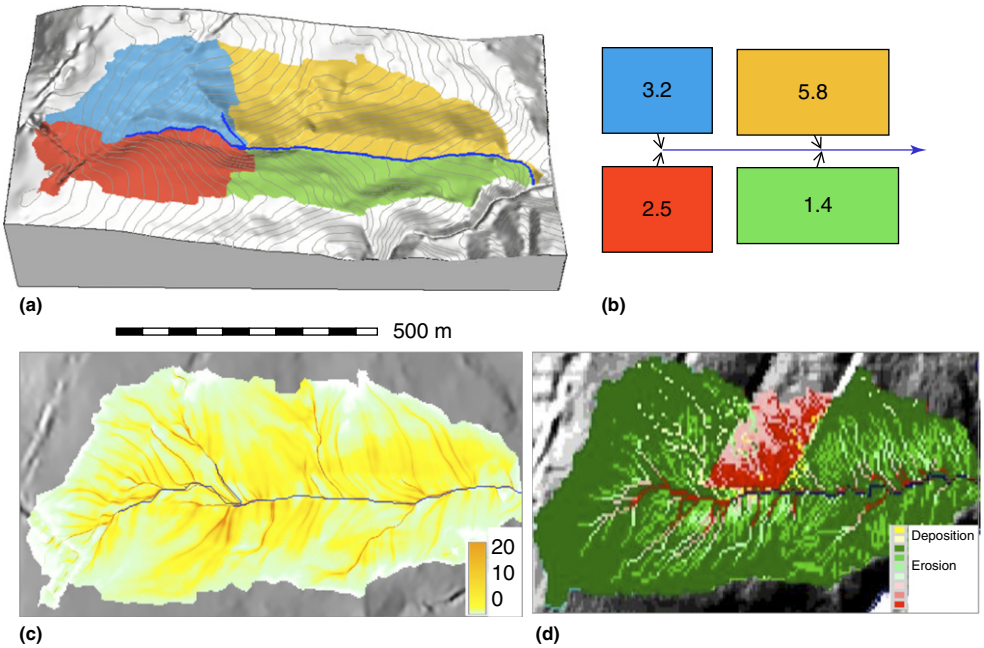

Figure 2 Representation of spatial variability: (a) spatially averaged representation: study area is partitioned into hydrologic units; (b) complex topography within hydrologic units is replaced by simple geometry of a tilted plane with uniform slope and soil erosion is estimated as uniform value within each unit; (c) spatially distributed representation estimates topographic erosion index for each grid cell using raster-based flow routing; (d) spatially distributed erosion and deposition rates estimated by GeoWEPP, red area shows high erosion rates due to vegetation removal (Moore et al., 2007).

single storm as well as an average long-term impact over several years.

3.9.2.4 GIS-Based Erosion Modeling

GIS implementation of erosion models supports efficient management of georeferenced data, computation of input parameters for different scenarios, spatial analysis of the modeling results, and effective visualization. GIS also incorporates tools for statistical analysis and modeling of erosion processes captured by remotely sensed data.

In early 1990s, Geographic Resources Analysis and Support System (GRASS) (Neteler and Mitasova, 2008) provided an environment for pioneering work in integrating GIS and hydrologic as well as erosion modeling (Rewerts and Engel, 1991; Mitchell et al., 1993). Most of the geospatial erosion modeling development and applications focused on agriculture, soil conservation, sediment pollution control, sustainable military land management (Harmon and Doe, 2001; Gaffer et al., 2008), and forestry, especially post-wildfire impacts.

Among the first implementations of hillslope erosion modeling within GIS was the computation of the Universal Soil Loss Equation (USLE) (Wischmeier and Smith, 1978), and derivation of its topographic parameters from digital elevation models (DEMs). Moore and Burch (1986) and later Moore and Wilson (1992) paved the way for the USLE applications for landscapes with complex topography by deriving the relationship between the unit stream power theory and USLE. Although the work generated heated discussions, it stimulated development in the direction that resulted in numerous implementations of USLE with GIS support for complex topographic conditions (Mitasova et al., 1996; Desmet and Govers, 1996). More recent GIS applications of USLE cover wide range of scales including large watersheds with land cover mapped from remote sensing imagery (Suri et al., 2002; Cebecauer and Hofierka, 2008; Pandey et al., 2009a, b; Jain and Das, 2010).

USLE and its updated, improved versions (Revised Universal Soil Loss Equation RUSLE and RUSLE2) have been used to estimate soil detachment within watershed-scale models that focus on nonpoint source pollution in agricultural, environmental, and engineering applications, including well known models such as ANSWERS, AGNPS, and SWAT (Rewerts and Engel, 1991; Mitchell et al., 1993; Lim et al., 2005; Kim et al., 2009). These models have been coupled with proprietary and open source GIS to process and manage modeling inputs and analyze the outputs (**Table 1**). Several watershed modeling systems have been recently implemented as on-line tools (Park et al., 2009).

Although USLE was developed as a simple tool for farmers to encourage soil conservation and thus its representation of erosion processes has been greatly simplified, the needs for research level modeling stimulated development of more complex models and their coupling with GIS. A process-based, continuous time model, based on the work by Foster (1982), was developed as WEPP (Flanagan and Nearing, 1995; Flanagan et al., 2007). Adaptation of WEPP to GIS, which led to the development of Geo WEPP (Renschler, 2003), traces the flow of sediment along flow paths on hillslopes generated from a DEM. Integration of water and wind erosion models

Table 1 Selected soil erosion models and their coupling with GIS; s, r – sheet and rill erosion; g – gullies; ch – channel; fl – fluvial; dz – elevation change; see also US Department of Agriculture, Agricultural Research Service (USDA ARS) at http://www.ars.usda.gov/Research/docs.htmdocid=5971, SWAT at http://swatmodel.tamu.edu/, EUROSEM at http://www.eurosem-soil-erosion.org/, LISEM at http://www.itc.nl/lisem/

Models	*Processes*	*Spatial scale and representation*	*Temporal scale*	*GIS implementation*	*Reference*
USLE	s, r	hillslope – profile	annual	map algebra	USDA ARS
RUSLE	s, r	hillslope – profile	annual – event	map algebra	USDA ARS USDA
GeoWEPP	s, r, ch	small watershed – raster	continuous time – event	extension, Web	ARS, NSERL USDA
AnnAGNPS	s, r, ch	watershed – custom grid	continuous time – event	custom GIS	ARS
ArcSWAT	s, r, ch	watershed – hydrologic unit	continuous time – event	extension	USDA ARS, TAMU
MapWinSWAT	s, r, ch	watershed – hydrologic unit	continuous time – event	custom Web GIS	USDA ARS, TAMU
openLisem	s, r, ch	watershed – raster	event	PCRaster	De Roo et al. (1996)
SIBERIA	s, r, ch, dz	landscape – raster	continuous time	data input	CSMDS (2011)
CHILD	s, r, ch, dz	landscape – mesh	continuous time	data input	CSMDS (2011)
USPED	s, r	small watershed – raster	annual – event	map algebra	Neteler and Mitasova (2008)
SIMWE	s, r	small watershed – raster	event	GIS module	Neteler and Mitasova (2008)
r.landscape.evol	s, r, ch, dz	landscape – raster	continuous time	GIS module	Barton et al. (2010a)

within the WEPP modeling framework is under development. It represents an important step toward understanding of combined impacts of water and wind erosion on soil conservation and agricultural sustainability.

Several erosion modeling systems with strong geospatial components have been developed in Europe. European Soil Erosion Model (EUROSEM) (Morgan et al., 1998) introduced a dynamic approach for predicting sediment transport from small watersheds. The LImburg Soil Erosion Model (LISEM) (De Roo et al., 1996; Sheikh et al., 2010) is a physically based runoff and erosion model for research, planning, and conservation purposes. It simulates the spatial effects of rainfall events on small watersheds and it uses the free GIS PCRaster Environmental Software (Karssenberg et al., 2001). As one of the most comprehensive geospatial erosion modeling tools, LISEM incorporates rainfall, interception, surface storage in microdepressions, infiltration, vertical movement of water in the soil, overland flow, channel flow in man-made ditches, detachment by rainfall and throughfall, transport capacity, and detachment by overland flow. Influence of compaction on the hydrological and soil erosion processes and gully incision are also included.

The SIMulation of Water Erosion (SIMWE) model (Mitas and Mitasova, 1998; Mitasova et al., 2005b) was developed as a bivariate generalization of hillslope erosion model used by WEPP to capture the spatial pattern of erosion, sediment transport, and deposition under spatially diverse conditions. Its robust path sampling algorithm and integration within GIS supports simulations of water and sediment flow patterns at high spatial resolutions, including impacts of small terrain variations such as depressions, ditches, or, checkdams.

Although several GISc-based implementations of erosion models predict locations of high erosion due to concentrated water flow, specific models that focus on ephemeral gully erosion were also developed (DeRose et al., 1998; Woodward, 1999). These models rely on field observations and modified channel sediment transport equations to improve the quantitative estimates of sediment eroded by ephemeral gully formation. Time series of aerial photography combined with multitemporal DEMs were also used to map the location, evolution and erosion rates of gullies (Martínez-Casasnovas et al., 2004).

In addition to the models focused on short term erosion (single event to multiple years), landscape evolution models have been developed to capture impact of erosion on landforms over hundreds or thousands of years. These models commonly use GIS data as inputs, but they have been developed and used mostly outside GIS and are covered in respective volumes of this series. Well known models include SIBERIA (Willgoose et al., 1991; Hancock et al., 2002; Willgoose, 2004), CHILD (Tucker et al., 2001a, b), or rule-based cellular automata models for simulation of landforms (Luo, 2001), braided rivers evolution (Murray and Paola, 1994) and sand dunes (Pelletier et al., 2009). The WILSIM landform evolution model (Luo et al., 2004) was implemented as a web-based simulation tool. Recently, the development of landscape evolution models has been coordinated by the Community Surface Dynamics Modeling System (CSMDS, 2011) program.

Statistical approaches have been commonly combined with remote sensing techniques to improve the results of erosion mapping. For example, a logistic regression-based erosion index was developed to map probability of erosion resulting from concentrated water flow from high resolution DEMs (Pike et al., 2009). Tree-based regression models were used to identify the topographic parameters that explain the variability in field gully measurements (Kheir et al., 2007). The most recent GIS-based models study pattern of erosion and deposition rates at very high resolutions using repeated scans of landscape by terrestrial LiDAR and by differencing the resulting DEMs.

Several recent papers indicate that "there are major weaknesses in the current understanding and data underpinning existing models" (Govers et al., 2007; Wainwright et al., 2008; Polyakov et al., 2004; Finlayson and Montgomery, 2003; Jetten et al., 2003). For example, Van Oost et al. (2005) concluded that performance of process-based erosion and hydrological models is extremely sensitive to parameter estimations and that predictions are generally poor. The difficulties associated with accuracy of spatially distributed soil erosion models are commonly due to the spatial and temporal variability of erosion processes and uncertainty associated with the model parameters. Jetten et al. (2003) suggest that model performance may be improved by using more complete spatial information

for model calibration and validation instead of the data restricted to the measurements at watersheds outlets. Spatially and temporally distributed observations may provide the data to elucidate the poorly understood interactions between sediment load and detachment rates, and provide insights into scaling of erosional processes and mechanisms. Therefore, adjustments to the theoretical foundations of erosion modeling presented in the next section can be expected in future as new monitoring and sensing technologies provide more complete experimental data and field observations.

3.9.3 Foundations in Erosion Modeling

Spatial and temporal patterns of erosion and deposition are results of complex interactions between the Earth system processes such as rainfall, surface, subsurface and ground water flow, vegetation growth, soil detachment, transport, and deposition. The focus of this section is on soil and sediment erosion and transport while treating rainfall, runoff, vegetation cover, and soil properties as inputs without going into detail about the estimation of these parameters' values. Here, general mathematical representation of erosion and sediment transport processes is described and relation between models with different levels of complexity and backgrounds is derived, highlighting the common principles.

3.9.3.1 Sediment Transport and Net Erosion/Deposition Equations

Soil, detached by raindrop impact and shearing force of overland flow is transported by flowing water until its transport capacity decreases, leading to sediment deposition (Haan et al., 1994). The fundamental relationship that governs sediment transport by overland flow is continuity of mass. It can be described by the sediment continuity equation, which relates the change in sediment storage over time, and the change in sediment flow rate along 3D hillslope to effective sources and sinks (Haan et al., 1994; Govindaraju and Kavvas, 1991; Foster and Meyer, 1972). To capture the spatial pattern of sediment transport over complex topography the bivariate form of the continuity of sediment mass equation (Hong and Mostaghimi, 1997) is used

$$\frac{\partial[\rho_s(x,y,t)h(x,y,t)]}{\partial t}+\nabla\cdot\mathbf{q}_s(x,y,t)=\text{sources}-\text{sinks}=d_s(x,y,t), \quad [1]$$

where (x, y) are georeferenced coordinates, t (s) is time, $\rho_s(x, y, t)$ (kg m^{-3}) is sediment mass density, $h(x, y, t)$ (m) is water flow depth, $\mathbf{q_s}(x, y, t)$ (kg (ms)$^{-1}$) is the vector that represents the direction and rate of sediment flow per unit width (unit sediment load), ∇ denotes divergence of the sediment flow vector field, and $d_s(x, y, t)$ (kg m^{-2} s^{-1}) is the net erosion or deposition rate. The sediment flow rate is a function of water flow and sediment concentration:

$$\mathbf{q_s}(x,y,t)=\rho_s(x,y,t)\mathbf{q}(x,y,t), \quad [2]$$

where $\mathbf{q}(x, y, t)$ (m^2 s^{-1}) represents the direction and rate of water flow per unit width (unit flow discharge vector) that can be expressed as a function of water depth $h(x, y, t)$, where the form of this function depends on the channel cross-section and flow conditions (Haan et al., 1994).

A simplified, steady state form of the continuity equation can be derived for the conditions when, at the given location, the change in water flow and sediment concentrations over time is close to zero. The net erosion or deposition rate $d_s(x, y)$ is then computed as a divergence of steady state sediment flow rate per unit width $\mathbf{q_s}(x, y)$:

$$\frac{\partial[\rho_s(x,y,t)h(x,y,t)]}{\partial t}=0 \quad \rightarrow \quad \nabla\cdot\mathbf{q}_s(x,y)=d_s(x,y). \quad [3]$$

Assuming steady rainfall excess rates, eqn [3] applies to the peak flow and peak concentration conditions when the water depth and sediment concentrations remain constant over time. To simplify equations, the (x, y) notation indicating spatially distributed variables represented by bivariate continuous functions is omitted in the rest of this chapter.

The sources and sinks term in eqn [1] is derived from the assumption that the detachment and deposition rates are proportional to the difference between the sediment transport capacity and the actual sediment flow rate (Foster and Meyer, 1972):

$$d_s=\sigma[T_c-q_s], \quad [4]$$

where T_c (kg(ms)$^{-1}$) is the sediment transport capacity, $q_s=|\mathbf{q_s}|$ is the magnitude of sediment flow rate per unit width, and σ (m^{-1}) is the first-order reaction term dependent on soil and cover properties. The expression for σ can be obtained from the following relationship (Foster and Meyer, 1972):

$$\frac{d_s}{D_c}+\frac{q_s}{T_c}=1 \quad [5]$$

which states that the ratio of the erosion rate to the detachment capacity D_c(kg m^{-2} s^{-1}) plus the ratio of the sediment flow rate to the sediment transport capacity is a conserved quantity (unity). Equation [5] is based on the observed relationship between soil detachment and transport when the finite amount of energy available in the overland flow is applied proportionally to detaching and to transporting the sediment so that the total relative available energy is unity (Haan et al., 1994). The σ coefficient thus controls how close is the sediment transport to the detachment limited (erosion only) or transport limited (maximum extent of deposition) regime (**Figure 3**). The detachment capacity D_c is then proportional to the transport capacity T_c:

$$D_c=\sigma T_c. \quad [6]$$

This leads to the expression of net erosion and deposition as:

$$d_s=D_c\left(1-\frac{q_s}{T_c}\right). \quad [7]$$

This concept is used in several erosion models including WEPP (Haan et al., 1994; Flanagan and Nearing, 1995) and SIMWE (Mitas and Mitasova, 1998). To estimate deposition of particles with different settling velocities σ may be

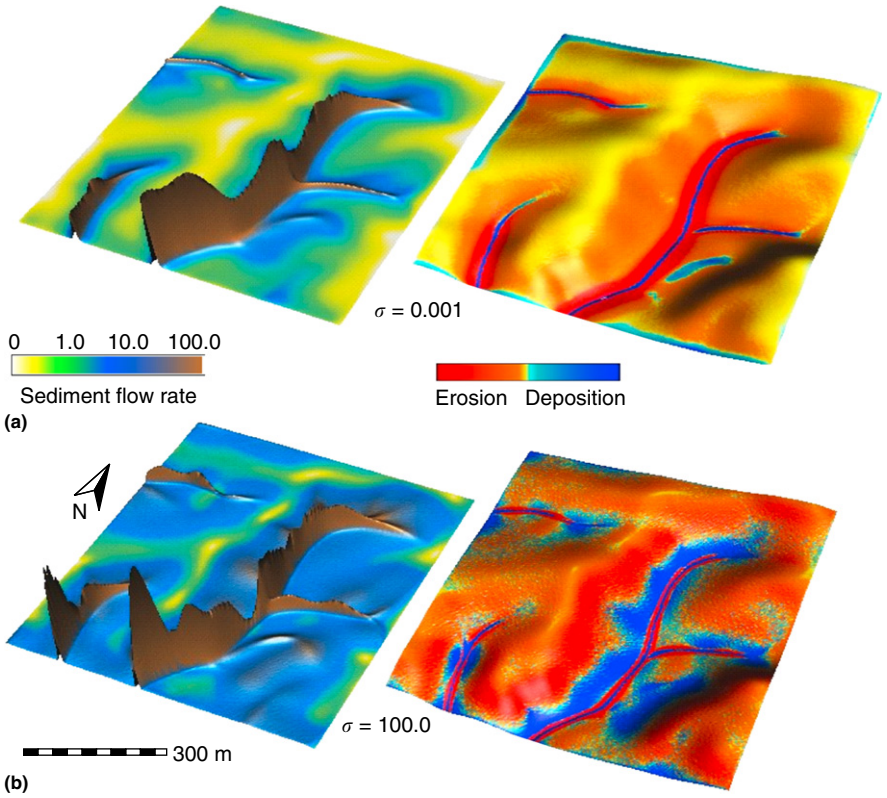

Figure 3 Impact of σ on spatial distribution of sediment flow rate (visualized as a surface) and erosion and deposition (draped as a color map over DEM): (a) low value of $\sigma=0.001$, with $D_c \ll T_c$ leads to prevailing erosion, close to the detachment limited regime, (b) high value of $\sigma=100$, $D_c \gg T_c$ leads to large extent of deposition, close to the transport capacity limited regime.

approximated by (Foster, 1982):

$$\sigma = \frac{V_s}{2q}, \quad [8]$$

where V_s (m s^{-1}) is settling velocity for the given particle size and q (m^2 s^{-1}) is flow discharge per unit width. It is possible to use other frameworks for estimation of σ. For example, Govers et al. (2007) proposed to express the detachment D_L as function of unit length sheer force G:

$$D_L = \alpha G\left(1 - \frac{q_s}{T_c}\right), \quad [9]$$

where α is an empirical coefficient.

It is important to note, however, that the relationship between the sediment detachment and transport capacities and the actual detachment and sediment loads is not fully understood (Govers et al., 2007; Nearing et al., 1997). Further experimental research is needed to elucidate this relationship and develop the underlying theory and equations.

3.9.3.2 Detachment and Sediment Transport Capacities

To solve the equation for sediment transport rate, it is necessary to estimate the transport and detachment capacities. The sediment transport capacity T_c and detachment capacity D_c represent the maximum potential sediment flow rate and the maximum potential detachment rate, respectively. Numerous simplified empirical equations represent these rates under different conditions (Julien and Simons, 1985). They are often expressed as functions of shear stress (Foster and Meyer, 1972):

$$T_c = K_t \tau^a, \quad [10]$$

$$D_c = K_d(\tau - \tau_0)^b, \quad [11]$$

where K_t(s) is the effective sediment transport capacity coefficient, K_d(s m^{-1}) is the effective erodibility (detachment capacity coefficient), τ(Pa=kg m^{-2}) is the shear stress, τ_0(Pa) is the critical shear stress, and a and b are empirical exponents. The shear stress τ is function of water depth h and surface slope angle β(deg) such that

$$\tau = g_w RS, \quad [12]$$

where $g_w=\rho_w g$ is the hydrostatic pressure of water with the unit height, $g=9.81$ (m s^{-2}) is the gravitational acceleration, $\rho_w=10^3$ (kg m^{-3}) is the mass density of water, $S=\tan\beta$ is surface slope and β (deg) is the steepest slope angle (see Haan et al. (1994), Moore and Burch (1986) for discussion on relationship between water depth and wetted perimeter used in the shear stress and stream power equations).

Transport capacity, especially in channels, streams and rivers, can be expressed as a function of unit stream power

ω (J (ms)$^{-1}$) (Moore and Burch, 1986) that represents the rate of energy dissipation against the bed and banks of a channel. If the stream velocity v (ms^{-1}) is estimated using Manning's equation (Haan et al., 1994; Dingman, 2002), then

$$v = n^{-1}h^{0.6}S^{0.5}, \quad [13]$$

where n is Manning's coefficient, then the unit stream power can be expressed as:

$$\omega = \tau v = g_w n^{-1} h^{1.6} S^{1.5}, \quad [14]$$

Sediment transport capacity is then computed as

$$T_c = K_s \omega = K_s n^{-1} g_w h^m S^n, \quad [15]$$

where K_s is transport capacity coefficient. Several studies indicate that stream power is a better hydraulic predictor variable for detachment and sediment yield than is shear stress (Nearing et al., 1997, 1999). The equation for sediment transport can significantly influence the magnitude and spatial pattern of sediment flow rates as well as the predicted erosion and deposition (**Figure 4**). Field observations are generally needed for selection of the sediment transport equation and its parameters that adequately represents the specific modeled landscape.

Julien and Simons (1985) analyzed numerous sediment transport equations and derived the following general equation

$$q_s = \varphi i^{\delta} q^m S^n (1 - \tau/\tau_0)^{\varepsilon}, \quad [16]$$

where q is unit water discharge, i is rainfall intensity, and φ, δ, ε, m, n are experimental or physically based coefficients that depend on type of flow.

When the critical shear stress τ_0 is negligible and for channels where $\delta = 0$ and q_s is not dependent on rainfall intensity the equation simplifies to

$$q_s = \varphi q^m S^n. \quad [17]$$

As presented above, the stream power, shear stress, and consequently transport and detachment capacities are generally expressed as power functions of water flow properties and slope. For a given rainfall excess rate and surface roughness, these two variables can be derived from DEM using the GIS functions for topographic analysis to compute the slope, and the flow routing tools to compute the upslope contributing area as an input for estimating unit water flow and water depth.

The parameters K_t, K_d, τ_0 used for the estimation of D_c and T_c are functions of soil and land-cover properties, and are much more difficult to estimate accurately than the topographic parameters. They have been derived using empirical equations or directly from experiments for a wide range of soils, cover, agricultural, and erosion prevention practices within the WEPP model (Flanagan and Nearing, 1995), but the values are valid only for the conditions similar to those in the experiments. Moreover, for landscape scale modeling, the soil data are rarely available at the level of detail comparable with DEMs, and temporal changes in soil properties are generally neglected. Land-cover data can be obtained at very high resolutions from airborne or even satellite imagery, however, the relationships between the type and density of vegetation cover and the soil detachment and transport parameters are not very well understood.

In addition to the difficulties of accurate estimation of detachment and transport capacity parameters, the values of exponents a, b in the eqns [10] and [11] or m, n in eqn [16] depend on the type of flow (Julien and Simons, 1985) and substantially influence model behavior. For example, the WEPP model uses $a = 1$ and $b = 1.5$ which means that with increasing water flow, transport capacity increases faster than detachment, which is not always the case. Uniform values of these exponents are commonly not general enough for erosion modeling at landscape scale with different types of flow due to variability in land-cover properties and spatially variable exponents may be needed (Mitas and Mitasova, 1998).

The solution of eqn [1] can be obtained by several partial differential equation solvers, including finite element methods (Hong and Mostaghimi, 1997), finite difference methods (Desmet and Govers, 1995), or path sampling (Mitas and Mitasova, 1998; Mitasova et al., 2005b). Detailed description

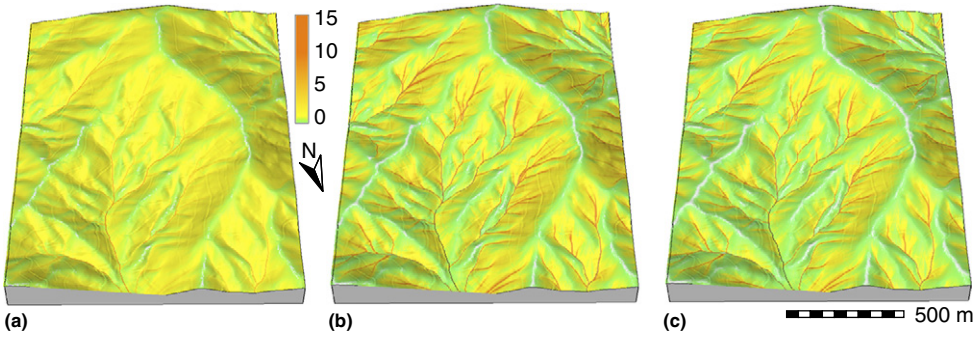

Figure 4 Impact of the sediment transport equation on spatial distribution of sediment flow rate: (a) shear stress eqn [10] with $a = 0.6$ predicts sediment transport increasing slowly with concentrated flow; (b) with $a = 1.5$ sediment transport increases rapidly with concentrated water flow; (c) stream power eqn [15] further increases the difference between sediment transport by sheet and concentrated flow.

of these methods is beyond the scope of this chapter, however, in the following sections, various simplifications of the full solution useful for GIS-based soil erosion modeling are described.

3.9.4 Simplified Models of Erosion Processes

To satisfy the need for models which are easy to compute and for which data are readily available, equations for simplified models of erosion processes can be derived. Depending on interactions between rainfall, runoff, and local soil and cover conditions, erosion and sediment transport varies between two limiting cases (Foster and Meyer, 1972; Tucker et al., 2001a):

- detachment capacity limited,
- sediment transport capacity limited.

Deriving equations for these limiting cases by simplifying the general sediment transport equation, leads to well-known soil erosion models that are useful for estimates of average annual soil erosion rates or total sediment loads at watershed outlets. In addition to the limiting cases of sheet and rill erosion, gully formation and a landscape evolution model that integrates several erosion processes are also discussed.

3.9.4.1 Detachment Capacity Limited Case

When transport capacity of overland flow exceeds its detachment capacity over the entire studied landscape, erosion, and sediment transport is detachment capacity limited (i.e., no deposition occurs). For example, this case is typical for sediment transported by large amount of water over compacted soil. The detachment capacity limited case is represented by $T_c \gg D_c$ leading to $\sigma \to 0$. Assuming that the critical shear stress is negligible $\tau_0 = 0$ the net erosion will be equal to the detachment capacity:

$$d_s \approx D_c = K_d \tau^b = K_d (g_w h S)^b. \quad [18]$$

This equation can then be used to compute the detachment limited, steady state erosion with water depth approximated, for example, from upslope contributing area. If more accurate estimate is needed, water depth distribution can be computed by a hydrologic model.

If the estimate of water depth is further simplified by assuming a planar hillslope with no water flow divergence or convergence, upslope contributing area per unit width can be replaced by hillslope length, leading to expression that is the basis for the most common erosion model USLE and its revised version RUSLE

$$D = RKLSCP, \quad [19]$$

where D (kg m^{-2} yr^{-1}) is average annual soil loss, R (M J mm (ha hr yr)$^{-1}$) is rainfall factor, K (ton ha hr (ha M J mm)$^{-1}$) is soil erodibility factor, LS is a dimensionless topographic (length-slope) factor, C is a dimensionless land-cover factor, and P is a dimensionless prevention measures factor. The length-slope factor has been derived from experiments and in the original USLE has the form (Wischmeier and Smith, 1978):

$$LS = (L/L_0)^m 64.5 \sin^2\beta + 4.56 \sin\beta + 0.0654, \quad [20]$$

where L (m) is the hillslope length, $L_0 = 22.1$ m is the length of the standard USLE experimental plot, m is exponent with values ranging between 0.2 for slopes less than 1% and 0.5 for slopes steeper than 5%. RUSLE expands the applicability of this equation by introducing additional empirical equations for computation of LS factor for different slope steepness intervals and provides updated values and equations for computation of all factors, including the R-factor for individual storms (Renard et al., 1994).

The USLE/RUSLE has been developed for estimation of average sheet and rill erosion on uniform fields with simple, relatively planar geometry. Numerous efforts and implementations have extended its applications to large watersheds and fields with complex topography. For example, USLE is used in several nonpoint source pollution models for estimation of averaged soil detachment in hydrologic units, with the detached soil then routed through the watershed.

An important modification of USLE/RUSLE has been derived by Moore and Burch (1986) and applied within GRASS GIS (Mitasova et al., 1996). This improvement replaced the hillslope length by upslope contributing area (**Figure 5**), leading to the following equation:

$$D = RKCP(m+1)\left(\frac{U}{L_0}\right)^m \left(\frac{\sin\beta}{S_0}\right)^n, \quad [21]$$

where D(kg m^{-2} yr^{-1}) is the average annual soil detachment (soil loss) rate, U(m^2 m^{-1}) is the upslope contributing area per unit width (a proxy for discharge), and $S_0 = 0.09$ is the slope of the standard USLE plot. Single storm and monthly R are also available, making eqn [21] suitable for estimation of soil loss for single storms and for modeling of monthly soil loss distribution over a year (Haan et al., 1994).

Exponents m, n depend on the prevailing type of erosion (sheet, rill) and the typical values are $m = 0.4$–0.6 and $n = 1.0$–1.3. Replacement of slope length, used in the original formulation of USLE/RUSLE, by the upslope area predicts increased erosion due to the concentrated flow without the need to *a priori* define these locations as inputs for the model.

It is important to note that the USLE/RUSLE model is commonly applied within GIS for conditions for which it has not been originally designed and at scales at which its validity is uncertain. For example, the original values of the USLE/RUSLE factors have been derived from experiments using plots only 22.13 m long, however, many published GIS applications of USLE used the equations at resolutions with much larger grid cell size and at locations with much steeper topography than the 9% slope of the USLE plots (Pandey et al., 2009a). The authors generally justify such applications by the fact that comparable experiments were not performed for the studied conditions and USLE was the best option available to them. Moreover, in complex topography, detachment limited erosion is rather rare because concave areas at toes of hillslopes reduce transport capacity, leading to sediment deposition, further limiting the applicability of the original USLE/RUSLE

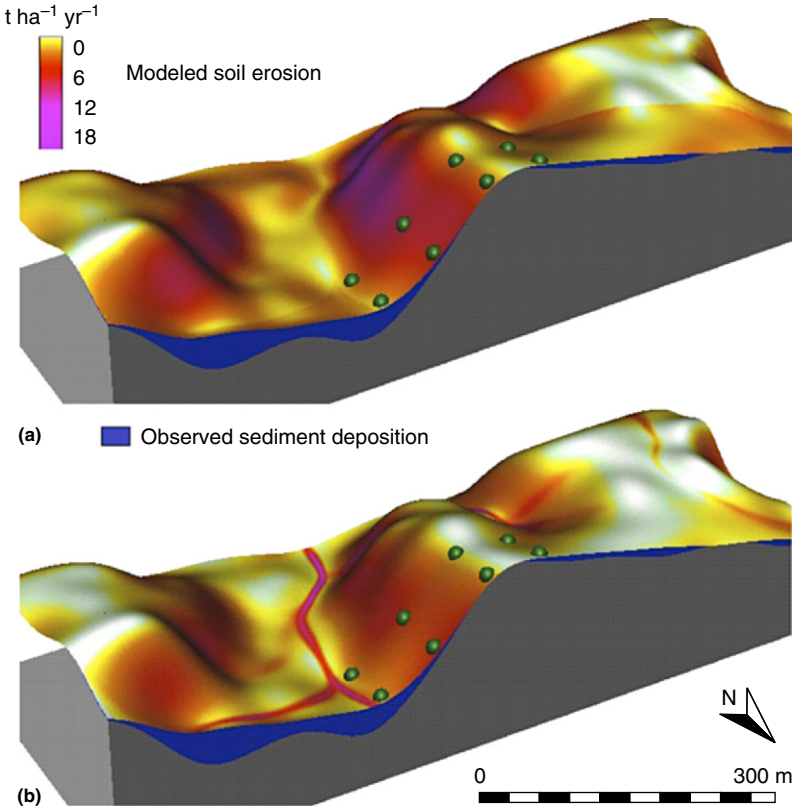

Figure 5 Spatial pattern of topographic erosion factor based on: (a) flowpath length (eqn [19]), which does not capture increased erosion due to convergent water flow, (b) flow accumulation (eqn [21]), which incorporates impact of water flow convergence. The topographic factor maps are draped over elevation surface. The cross-section shows observed deposited material, indicating locations where these topographic erosion factors are not applicable for modeling long term net erosion/deposition pattern. Images based on data provided by Prof. K. Auerswald, Technische University Muenchen.

(Figure 5). In spite of its limitations, the USLE/RUSLE models, as well as their modifications and applications in GIS have played an important role in soil conservation efforts and sustainable land management (Renard et al., 1994; Haan et al., 1994; Hammad et al., 2004; Cebecauer and Hofierka, 2008).

3.9.4.2 Transport Capacity Limited Case

If the soil detachment significantly exceeds the sediment transport capacity of overland flow, the sediment flow rate will be at the sediment transport capacity. This means that the magnitude of sediment flow can be approximated by T_c and net erosion/deposition rate can be computed as a change in the sediment transport capacity derived from eqn [3]:

$$d_s = \nabla \cdot \mathbf{q}_s \approx \nabla \cdot (T_c \mathbf{s}_0) = \frac{\partial (T_c \cos\alpha)}{\partial x} + \frac{\partial (T_c \sin\alpha)}{\partial y}, \qquad [22]$$

where $\mathbf{s}_0 = (\cos\alpha, \sin\alpha)$ is the unit vector in the steepest slope direction given by α(deg), the aspect angle of the terrain surface equivalent to the direction of flow. As opposed to the detachment capacity limited case, the transport capacity limited formulation can predict spatial pattern of both erosion and deposition (Figure 6).

The transport capacity limited case with spatially variable soil and cover properties can be modeled using the idea originally proposed by Moore and Burch (1986). It combines the USLE/RUSLE parameters and upslope contributing area per unit width to estimate the sediment flow at sediment transport capacity:

$$q_s \approx T_c \approx RKCPU^m (\sin\beta)^n. \qquad [23]$$

The net erosion/deposition d_s(kg m^{-2} s^{-1}) is then computed as a divergence of sediment flow vector field given by eqn [22].

The exponents m, n control the relative influence of water and slope terms and reflect the impact of different types of flow. The observed extent of colluvial deposits indicated that an exponent $m = 1$ reflects the pattern of compounded, long term impact of both rill and sheet erosion (Mitas and Mitasova, 1998). Averaging over a long-term sequence of large and small events was important for capturing the observed spatial extent of deposition as well as channel incision due to concentrated flow (Warren et al., 2005). Spatially variable $m(x, y)$, $n(x, y)$, approximated by a continuous function, can be used to account for the differences in surface flow (Figure 7).

Models representing limiting cases of erosion are simple to compute in a GIS using the standard flow routing,

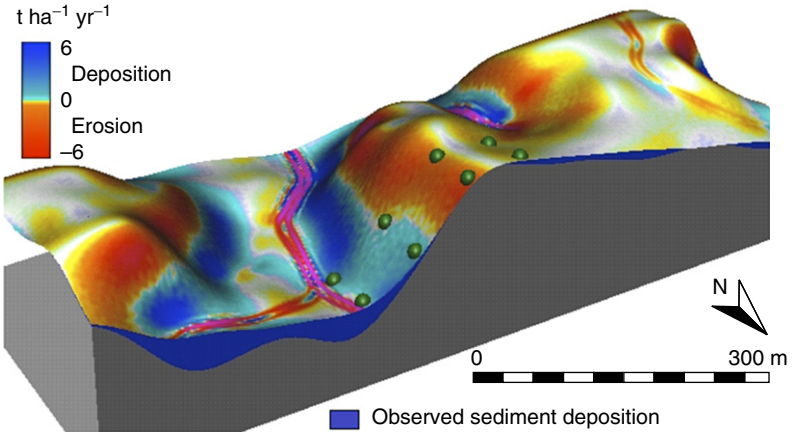

Figure 6 Topographic potential for net erosion and deposition, estimated as a change in sediment transport capacity.

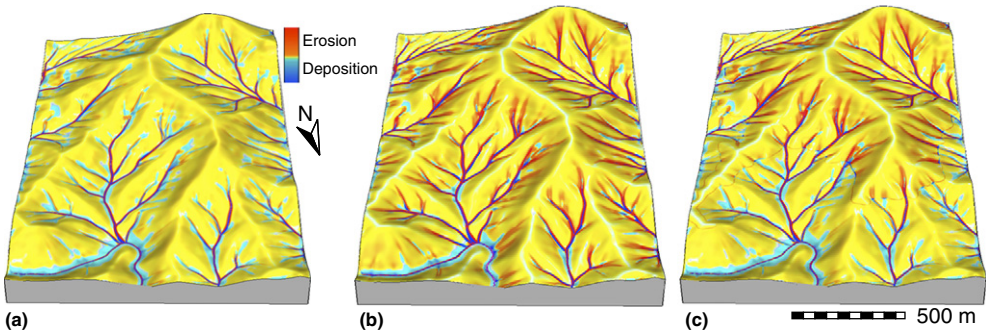

Figure 7 Impact of exponents m, n in eqn [23] on resulting erosion and deposition rates pattern: (a) $m=1.0$, $n=1.0$ predicts erosion in 87% and deposition in 13% area, including deposition in concave forms of headwaters; (b) $m=1.6$, $n=1.0$ predicts erosion in 92% area whereas limiting deposition to 8% area mostly in low, broader concave forms; (c) spatially variable $m=1$ at lower and $m=1.6$ at higher elevations.

topographic analysis modules combined with map algebra. They can be used to estimate spatial distribution of soil detachment and net erosion/deposition rates for a single storm, as well as monthly and annual averages. Caution should be used when interpreting the results from modifications of USLE/RUSLE that incorporate water flow convergence/divergence and erosion/deposition, because the soil and cover parameters were developed for simple planar fields and detachment limited erosion. To accurately predict erosion and deposition rates for complex terrain and spatially variable land-cover conditions these models need to be calibrated for a specific geographic area.

3.9.4.3 Process-Form Relationship

As shown in the section 3.9.4.2 topography controls the spatial pattern of sediment transport and erosion/deposition through upslope contributing area and slope angle. In this section, the role of terrain curvature in distribution of erosion and deposition is demonstrated.

Most sediment transport models route sediment in single direction along flow paths and compute the net erosion and deposition as a difference between sediment inflow and outflow along the segments of this path (Moore and Wilson, 1992; Desmet and Govers, 1995; Mitasova et al., 1996). Assuming uniform rainfall, soil and cover conditions, and a transport capacity limiting case with $q_s \approx T_c$, the net erosion/deposition rate along a flow path (univariate model) can be derived as directional derivative of sediment transport capacity in the direction of steepest slope (aspect):

$$d_s = \frac{\mathrm{d}T_c}{\mathrm{d}s} = \nabla T_c \cdot \mathbf{s}_0 \qquad [24]$$

$$d_s = K_e(\nabla h \cdot \mathbf{s}_0 \sin\beta - h\kappa_p), \qquad [25]$$

where $\kappa_p(\mathrm{m}^{-1})$ is profile curvature that measures the rate of change in slope in the gradient direction, $K_e = K_t\, \rho_w\, g$, and $d_s > 0$ represents the net erosion rate and $ds < 0$ represents the net deposition rate. The univariate formulation includes the impact of water flow convergence/divergence through the water depth term and flow acceleration/deceleration through the profile curvature.

Within the bivariate formulation, given by eqn [22], the net erosion and deposition rate is estimated as a divergence of

the sediment flow vector field $\mathbf{q}_s$ (Mitas and Mitasova, 1998):

$$d_s = \nabla \cdot \mathbf{q}_s = \nabla \cdot (T_c \mathbf{s}_0) \quad [26]$$

$$d_s = K_e[\nabla h \cdot \mathbf{s}_0 \sin\beta - h(\kappa_p + \kappa_t)], \quad [27]$$

where κ_t (m^{-1}) is the tangential curvature that measures the change in aspect (curvature in the direction perpendicular to the gradient, i.e., the direction tangential to a contour line projected to the normal plane).

When eqns [25] and [27] are compared, the fundamental difference is in incorporation of tangential curvature. According to the bivariate eqn [27], the spatial distribution of erosion/deposition is controlled by the change in the overland flow depth ∇h and by the local geometry of terrain including both profile and tangential curvatures. Equation [27] thus demonstrates that the local acceleration of flow in both the gradient and tangential directions play equally important roles in spatial distribution of erosion/deposition.

The impact of the tangential curvature is therefore twofold (Figure 8). First, κ_t influences the water depth through its control of water flow convergence and divergence, with tangential concavity leading to rapid increase in water depth and increase in erosion rates. Second, κ_t causes a local change in sediment flow velocity with an opposite effect, with tangential concavity reducing the sediment transport, creating conditions for deposition. Therefore, it is the interplay between the magnitude of water flow change and both terrain curvatures in eqn [27] which determines whether erosion or deposition will occur.

When the results of the univariate and the bivariate models were compared with the observed pattern of deposits (Mitas and Mitasova, 1998), the model that computes the sediment load change along a flowline (eqn [25]) failed to predict deposition observed in areas where $\kappa_p \approx 0$ but $\kappa_t < 0$.

The prediction by eqn [27] was in better agreement with the observed pattern of deposition in these areas (Figure 8). It is important to note, however, that the total sediment load at the outlet is the same for both formulations and it is only the spatial pattern of sediment redistribution within the watershed that is influenced by the univariate versus bivariate solution.

3.9.4.4 Path-Sampling Transport Modeling

Evolution of sediment transport over complex landscapes can be simulated using a path-sampling approach (Mitas and Mitasova, 1998; Mitasova et al., 2005b) that is based on the concept of duality between discrete particles and continuous fields. The approach solves the steady state sediment flow eqn [3] that is rewritten to include a small diffusion term $\propto \nabla^2\rho$:

$$-\frac{\gamma}{2}\nabla^2\rho + \nabla \cdot (\rho \mathbf{v}) + \rho\sigma|\mathbf{v}| = \sigma T_c, \quad [28]$$

where $\rho = \rho_s h (\mathrm{kg\,m^{-2}})$ is the mass of sediment carried by water per unit cross-section area, $\gamma (\mathrm{m^2\,s^{-1}})$ is the diffusion constant, and $\boldsymbol{v} (\mathrm{m\,s^{-1}})$ is the water flow velocity estimated by Manning or Chezy equation (Dingman, 2002). On the left hand side of eqn [28] the first term describes local diffusion, the second term is a drift driven by the water flow whereas the third term represents a velocity dependent 'potential' acting on ρ. The size of the diffusion constant is about one order of magnitude smaller than the reciprocal Manning's constant so that the impact of the diffusion term is relatively small.

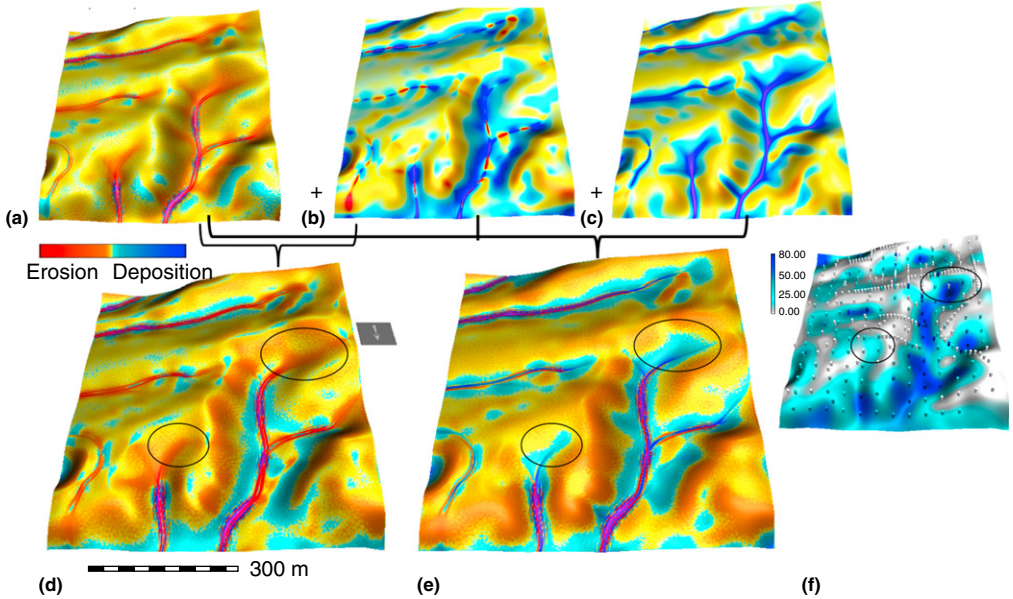

Figure 8 Computing net erosion and deposition using univariate and bivariate formulation (eqns [25] and [27]): (a) term representing change in water-flow depth ($\nabla h \cdot \mathbf{s_0} \sin\beta$); (b) term that combines water-flow depth with profile curvature ($h\kappa_p$); (c) term that combines water-flow depth with tangential curvature ($h\kappa_t$); (d) net erosion/deposition computed as a change in sediment flow along flow-path is a sum of (a) and (b); (e) net erosion/deposition as sediment flow divergence is a sum of (a), (b) and (c); (f) observed deposited sediment with highlighted locations where divergence improves the modeling result. Figure based on Mitas and Mitasova (1998) using data provided by Prof. Auserwald, Technical University Muenchen.

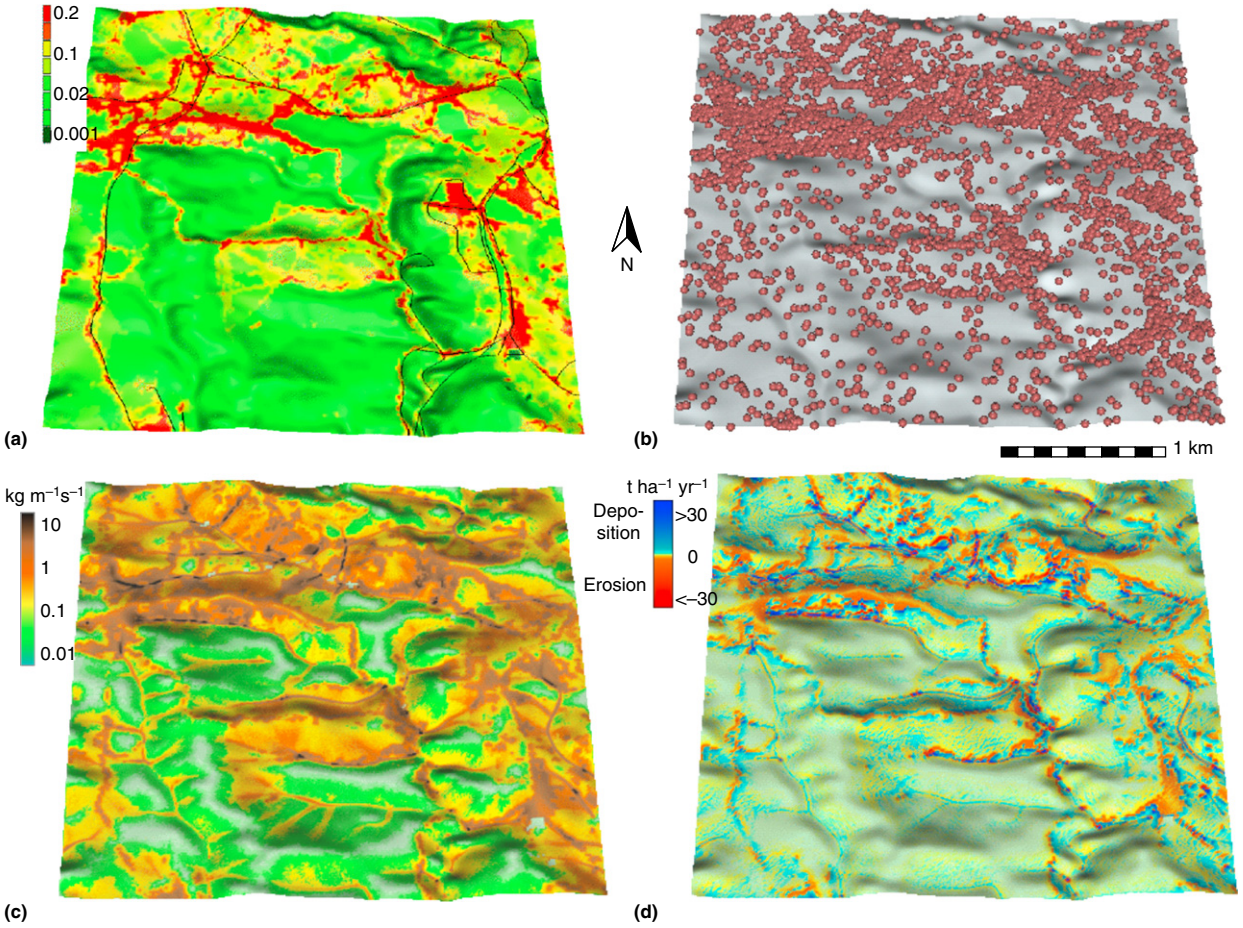

Figure 9 GIS-based erosion modeling using path sampling method: (a) C-factor at the study site with disturbed land shown in red; (b) particle representation of soil detachment (only 1% of particles is displayed), particle density is higher in locations with disturbed land; (c) raster representation of sediment flow rate computed as a function of particle density per grid cell; (d) net erosion and deposition computed as a divergence of sediment flow.

It represents local dispersion processes caused by micro-topography which is not captured by the DEM.

The sediment flow described by eqn [28] can be solved by the path-sampling stochastic method (Mitasova et al., 2005b) by propagation of particles according to the continuity equation. Sediment concentrations are then computed based on particle density (**Figure 9**). This approach has been used to develop the SIMWE model which was implemented in GRASS GIS as a module 'r.sim.sediment' (Neteler and Mitasova, 2008).

3.9.4.5 Gully Erosion

Traditionally, modeling of gully and channel erosion has been performed outside of a GIS because most of the required data, especially the DEMs, did not have sufficient resolution to capture the gully or channel geometry. With high resolution DEMs (submeter grid cell size) now available, gully and channel erosion models can be implemented and applied using GIS-based approaches.

Gullies develop under specific conditions when the tractive force of the water flow exceeds a certain threshold value and shallow flow starts to concentrate in the channel. This transition occurs abruptly at a knickpoint or headwall. In fact, several such transitions may occur, eventually merging the knickpoints and forming one incised channel (Haan et al., 1994). The gully then develops via headwall migration and channel widening. The process of initiation requires a relatively large rainfall event so that the rainfall excess generates water flow exceeding the threshold value needed to detach and transport large amounts of sediment. The immediate morphological effect of the gullying process is a substantial change in topography with a sharp change in slope in a headwall and channel banks. This contributes to a further gully development until a new equilibrium is found.

The difference between modeling the rill and gully erosion lies in the treatment of elevation represented by a DEM. In the case of landscape-scale rill erosion modeling, the elevation surface is considered as fixed throughout the erosion event. Actual net erosion/deposition rates change the elevation surface only marginally and the morphological effect can be observed only after many similar events. Gully erosion, however, has an immediate effect on topography and the elevation change must be taken into account during the simulation.

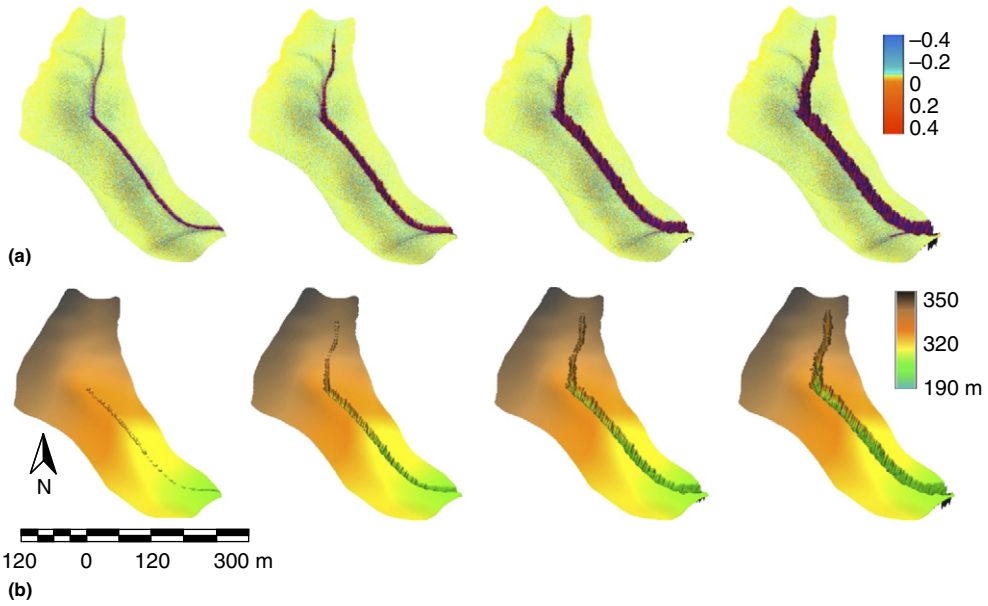

Figure 10 Temporal evolution of a gully, modeled in GRASS GIS: (a) elevation surface with evolving gully, color indicates spatial pattern of erosion/deposition rates in (kg m^{-2} s^{-1}), (b) evolving elevation surface: creation of multiple knickpoints, incision of the channel, upslope headwall migration and channel widening, color represents the elevation values in (m).

This inherently requires a dynamical erosion model reflecting the changes in topography. To simulate the gully formation, it is assumed that erosion starts before water flow reaches steady state, the sediment transport is close to detachment limited conditions, and all eroded material is transported outside the gully. Using eqn [1] to estimate erosion rates at time t(s) driven by the unit water flow q_t (at nonsteady state for the time steps $t_0, t_1, \ldots, t_s$, where t_s is time of concentration) the change in elevation $\Delta z(x, y, t)$ (m) due to net erosion can be estimated as

$$\Delta z(x,y,t) = \Delta t \cdot d_s(x,y,t)/\rho_s, \qquad [29]$$

where ρ_s(kg m^{-3}) is soil density and $\Delta t = t_i - t_{i-1}$ is the time interval. Using the map algebra in a GIS, the initial DEM_0 is modified using the changes in elevations $\Delta z(x, y, t)$. A new set of topographic parameters is then derived from the updated DEM_i to reflect new flow gradients used by the water flow and soil erosion model in the next iteration. **Figure 10** shows a time-series of a developing gully modeled by the SIMWE model (Mitasova et al., 2005b) in a GRASS GIS environment (Koco, 2009). It illustrates creation of multiple knickpoints, incision of the channel and then an upslope headwall migration and channel widening.

3.9.4.6 Statistical Modeling

As previously shown, even the physics-based erosion models require a set of empirical parameters that are derived from field or laboratory experiments using statistical methods. Statistical modeling can also be used to derive empirical models or indices that relate landscape surface attributes to erosion rates. The resulting models require field or remotely sensed data and are applicable only to locations with conditions similar to those for which they have been developed. For example, Pike et al. (2009) used logistic regression and neural networks to derive a probabilistic model that predicts the occurrence of channel erosion using the index P_e:

$$P_e = (1 + \exp^{-[-3.63+1.11LS+0.217w-12.1\kappa_h]})^{-1}, \qquad [30]$$

where LS is the estimated length-slope factor, w is the topographic wetness index, and κ_h is the plan curvature (tangential curvature projected to horizontal plane). Because this is an empirical model, the authors make it clear that the model should only be applied if the same methods were used to create the DEMs and calculate terrain attributes as in their application.

An alternative statistical approach explored the capabilities of three tree-based regression models to explain gully erosion field measurements using topographic parameters. The investigated parameters included elevation, upslope contributing area, aspect, slope, plan, profile, and tangential curvature; flow direction, flow width, flow path length, rate of change of specific catchment area along the direction of flow, steady-state, quasidynamic topographic wetness; and sediment transport capacity (Kheir et al., 2007). The best regression tree model combined the steady-state topographic wetness and sediment transport capacity indices, which explained 80% of the variability in field gully measurements.

3.9.4.7 Landscape Evolution Modeling

Most GIS-based erosion models focus on mapping the spatial pattern of erosion and deposition without taking into account changes in elevation surface. Landscape evolution models simulate erosion processes including their impact on elevation

surface and their feedback on erosion and deposition patterns. Landscape evolution process can be described by partial differential equations (Willgoose, 2004) and most models are implemented outside a GIS using customized code or numerical modeling environment such as MATLAB. An exception is a landscape evolution model that simulates impact of land use and climate change on landscape evolution *r.landscape.evol* that has been fully integrated with GRASS GIS (Barton et al., 2010a).

Simulation of landscape evolution over long periods of time requires integration of several erosion processes. These include change in elevation surface due to gravitational hillslope erosion modeled using diffusion equation, processes induced by surface water flow, including hillslope erosion and deposition, gully erosion, channel incision, and meandering in regions with low topography.

An approach inverse to the forward landscape evolution modeling was used to reconstruct ancient topography (Peeters et al., 2006) by computing soil erosion and deposition based on change in sediment flow rates estimated from slope and unit contributing area. Then, the topography was iteratively updated back in time by adding the elevation associated with erosion rates and subtracting elevation in areas with deposition. Comparison with field measurements of historical soil erosion and sediment deposition volumes shows that it is possible to simulate realistic soil redistribution patterns. Further research is necessary, however, to address simulation artifacts produced by the routing and elevation change computation used in this study (Peeters et al., 2006).

Several papers suggest the importance of large events in landscape evolution (Peeters et al., 2006; Mitasova et al., 1999) when long periods of relatively small events, dominated by transport capacity limited erosion and deposition, are disrupted by rare large events that cause flushing of deposits and transport of sediment over large distances. These large events are generally associated with gully and channel incision leading to significant changes in elevation surface.

3.9.5 GIS Implementation

Implementation of the simple erosion models in GIS is relatively straightforward and involves creating a workflow that includes input data processing, model computation, and analysis of results. The workflows can be developed using model builders available in GIS and saved in the form of scripts that support fully automated simulations. Complex physics-based models usually require partial differential equation solvers and can be fully integrated with GIS using the system's libraries for managing the geospatial data. More often, such models are only loosely linked to GIS.

3.9.5.1 Coupling GIS and Models

Erosion modeling can be coupled with GIS through data exchange, graphical user interface (GUI), or it can be fully integrated as set of modules or scripts (Mitasova and Mitas, 2002).

'Loose coupling' links a model with GIS through import and export of data. The model is developed independently from a GIS and different GIS software packages can be used for data preprocessing, analysis, and visualization of modeling results. Standardization in georeferenced data formats and improvements in software interoperability have made loose coupling a routine procedure. Several landscape evolution and erosion models are available with this type of GIS coupling (CSMDS, 2011).

'Tight coupling' integrates a model and a GIS using shared GUI which guides the user through input data processing, modeling, and analysis. The interface also allows the user to visualize the results using both the GIS display tools and specialized graphical and numerical outputs. This type of integration has proven to be effective for hydrologic and nonpoint source pollution modeling systems (Rewerts and Engel, 1991; Renschler, 2003; Di Luzio et al., 2002) and several models have been coupled with more than one GIS. Increasingly, the interface is provided through on-line tools via the Web Processing Service (WPS).

'Full integration' involves spatial models which are useful for a wide range of GIS applications. These models are developed and implemented within a GIS, using its programming tools such as Application Programming Interface (API), scripting language, or map-algebra operations. The spatial model is then run as a GIS function or command, with the inputs and outputs stored in a GIS database (no data transfer is needed). Portability of the model is restricted, and the enhancements as well as the maintenance of the model is dependent on the GIS. This type of model development is further supported by customization and application of development tools, extensions to map algebra (Wesseling et al., 1996) and visual modeling tools.

Full GIS integration of complex models involving solutions of coupled partial differential equations has been limited, in spite of several successful implementations (Mitas and Mitasova, 1998). Even with all the necessary capabilities available in the GIS, the biggest disadvantage of full integration of complex models is that the models become too dependent on the development and fate of a particular GIS. Changes in the GIS data structures, functionality, interface, libraries or programming tools, may require time consuming changes in the models or the models become incompatible with the latest version of the GIS software. Also, the fully integrated model is less portable and users have to install entire GIS even if they need the model only for a one-time application. Some of these issues have been addressed by open source software and community systems development.

Large, professional modeling systems, most commonly aimed at engineering applications, use both loose coupling with a GIS and their own, specialized GIS capabilities. An external GIS is generally used for storing, managing, and processing of basic topographic data and for generating the cartographic output. The modeling system itself includes support for GIS functions where tight coupling with the model is necessary, such as the design of a conceptual model for the given site, adjustment of finite-element grids and meshes, as well as modifications of the model parameters (conditions of simulations) based on the simulation results.

With the explosive growth of the Internet, erosion models useful for a wider range of users, such as farmers, land owners, city planners, or public land managers are being implemented as web-based applications. The successful applications include

not only the modeling tools, but also the databases with input data and model parameters so that the user does not have to deal with the time consuming tasks of finding, processing, and submitting the input data for the model runs. Generally, only selection of the location and land-use management scenario is needed from the given set of options. Spatial data are stored in a GIS on the server and the digital maps or animations, representing the inputs and model results, are served using the online map serving technology (Park et al., 2009; Luo et al., 2004).

3.9.5.2 Derived Model Parameters

Finding, importing, integrating, and processing the data necessary for erosion modeling can be a time-consuming task. Therefore, a well maintained, consistent GIS database makes data preparation for modeling and generating alternative scenarios highly efficient. The following input data are generally required for GIS-based erosion modeling.

Elevation data are widely available as raster DEMs. Accurate flow routing and slope estimation requires resolutions with grid size of 10 m and smaller and vertical precision at least in centimeters. If a raster DEM is not available, contours, or point data, such as LiDAR point clouds, can be interpolated to create the DEM (*see* Chapter 3.6). Elevation data are used to compute slope, direction of flow, and upslope contributing area for physics-based models as well as numerous other parameters such as curvatures or wetness indices for statistical models (*see* Chapter 3.7).

Land cover data are generally derived from aerial or satellite imagery as a raster map layer (*see* Chapter 3.4). If raster data are not available, polygon areas can be transformed to raster at desired resolution. Land cover data are used to estimate the land-cover *C*-factor for USLE and for surface roughness, detachment capacity and sediment transport capacity coefficients in process-based models. These parameters have empirically derived values and are commonly available in literature and reference tables (Haan et al., 1994).

Soil data are generally available as polygons and have to be transformed to raster or hydrologic units using standard GIS data model transformations. If soil samples are available, spatial interpolation using geostatistics methods is applied to compute the raster representation of soil properties that are the basis for computation of erosion related factors. Soil data are used to derive the soil erodibility *K*-factor for USLE and detachment capacity and sediment transport capacity coefficients in process-based models.

Rainfall data are available in the form of isoline maps for *R*-factor or from databases used for RUSLE. For field and small watershed scales, a single value is sufficient; for regional modeling the rainfall factor should be given as raster map and can be obtained using Tropical Rainfall Mapping Mission data (*see* Chapter 3.1). Rainfall factors can also be derived from measured rainfall data (Haan et al., 1994).

3.9.5.3 Analysis and Visualization

A GIS provides powerful tools for analysis and communication of modeling results, and it is commonly combined with advanced statistical packages and specialized tools to perform model calibration and validation. Erosion and sediment transport modeling involves substantially more uncertainty than modeling in disciplines where most experiments are done in laboratory under controlled conditions. Model calibration and validation are, therefore, an important component of the modeling effort and are generally handled by external statistical tools loosely coupled with models and GIS (Poeter et al., 2005). Calibration of erosion models and validation of the modeling results has been commonly limited by difficulties of data collection. Recent advances in temporal acquisition of high-resolution airborne or terrestrial LIDAR data provide new opportunities to test the accuracy of predicted patterns of erosion and deposition based on DEM differencing. This, in turn, can be used to evaluate the sensitivity of model parameters for obtaining accurate erosion magnitudes and distributions.

In addition to summary statistics, maps representing spatial distribution of soil detachment, net erosion and deposition, and sediment transport rate are among the most important outputs of erosion modeling that communicate the spatial pattern of sediment sources, highlight high erosion risk areas and locations with damaging rates of deposition. Perspective views of erosion modeling results draped over DEMs are especially effective in highlighting the relationship between landforms and the spatial pattern of erosion and deposition (**Figures 3** and **8**). Although the perspective 3D views of topography do not replace an accurate 2D map, they are useful in interactive mode for visual analysis of complex spatial relations. As static images, they can be used to improve the perception of 3D features and their impact on erosion that may be difficult to capture by 2D maps. Animations are commonly used to represent the process dynamics and this can include animated 2D images as well as dynamic surfaces in perspective 3D views (Mitas et al., 1997).

Recent advances in human–computer interaction technology provide environments for enhanced, collaborative exploration of landscape models. In addition to multitouch screens and immersive 3D environments, interaction with 3D objects is emerging as a powerful tool for investigation of landscape properties and processes. The Tangible Geospatial Modeling System (TanGeoMS) couples a 3D laboratory laser scanner and a physical landscape model with a video projector and GIS to support exploration of terrain change impacts on topographic parameters and land surface processes (Mitasova et al., 2006; Tateosian et al., 2010). The flexible clay landscape model can be modified by multiple users. When a modified landscape is scanned, the selected terrain parameter or process simulation is recomputed based on the scanned data and the result is projected over the modified surface (**Figure 11**). The projected image or animation provides the users with feedback on impact of their terrain modifications and guides the future exploration.

3.9.6 Case Studies

Two case studies were selected to illustrate the GIS-based erosion modeling and highlight its focus on spatial patterns of erosion and deposition.

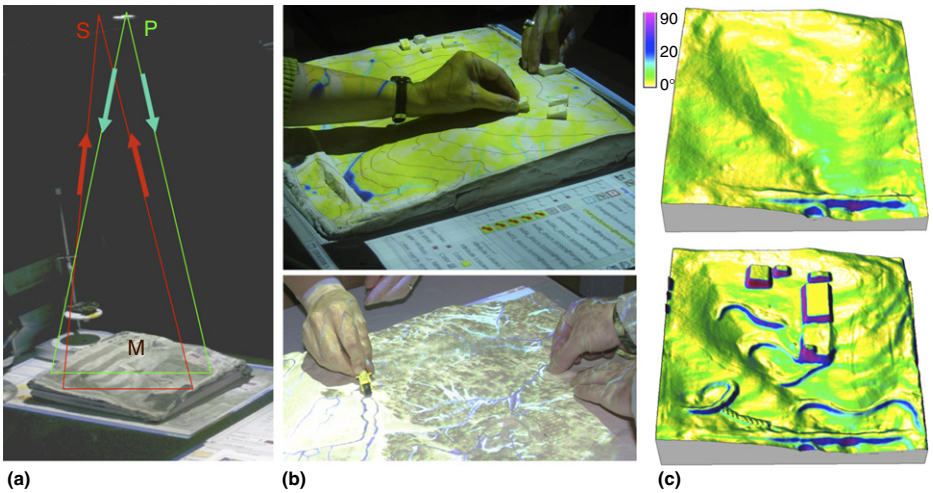

Figure 11 Tangible Geospatial Modeling System: (a) flexible landscape model M is scanned by an overhead 3D laser scanner S while GIS data (e.g., orthphoto) and simulation results are projected over the model using a projector P; (b) several users can modify the landscape model by adding buildings or creating road tracks; (c) perspective views of initial and modified landscape models; slope maps draped over the DEMs provide feedback on the modification impact on slope angle values.

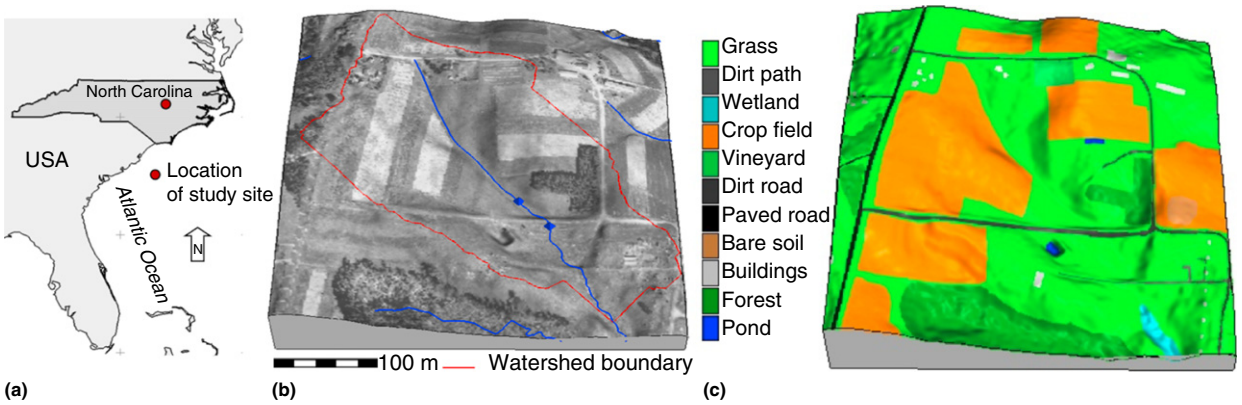

Figure 12 Case study site: (a) location in the central North Carolina, (b) aerial photo draped over DEM with watershed boundaries and two monitoring sites, and (c) simplified land cover used in simulations.

3.9.6.1 North Carolina Piedmont

A small watershed at the North Carolina State University Sediment and Erosion Control Research and Education Facility (SECREF) (McLaughlin et al., 2001) has been used for erosion model testing and sediment transport monitoring (**Figures 12** and **13**). This site is used to demonstrate advantages and limitations of various approaches to GIS-based erosion modeling. The 9.4 ha watershed has a mean slope of 3.4° and a maximum flow-path length of 530 m. The soil type is mostly Cecil, and land use includes agricultural fields, grass, small forested area, vineyard, buildings, and experimental ponds. Disturbances are limited to tilling at a 6 ha agricultural field.

The area was mapped by airborne LiDAR in the year 2001 with point density of 1 point for each 2 m resolution grid cell. Bare-ground points were used to compute a 1 m resolution DEM, a slope, and a direction of flow maps using regularized smoothing spline with tension (RST) method (Mitasova et al., 2005a). Several approaches were tested for mapping of flow accumulation and estimation of unit water flow, including single direction flow routing with 8 directions (SDR-D8 implemented in the GRASS module *r.watershed*), single direction flow routing with infinite number of directions (SDR-Dinf, module *r.flow*), and multiple direction flow routing with 8 directions (MDR-D8 module *r.watershed* and *r.terraflow*). Additional parameters for the erosion models were derived from land-cover, soil and rainfall data stored in a GIS and in the related WEPP databases.

Baseline erosion modeling was performed for simplified land cover (**Figure 12(c)**) to obtain estimates of soil erosion and deposition using the following models:

- on-line version of GeoWEPP to estimate runoff and sediment yield;
- GIS based version of detachment limited erosion model to estimate soil detachment;
- GIS based erosion/deposition model to estimate net erosion and deposition rates;
- overland water flow and sediment transport model SIMWE to estimate runoff and sediment flow rates;

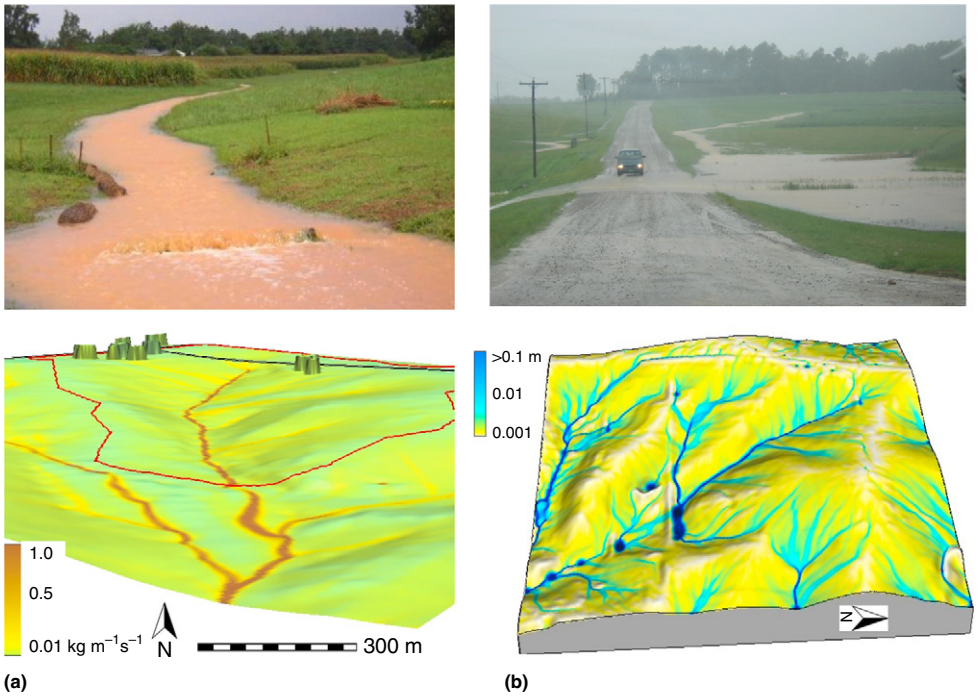

Figure 13 Study site after high intensity storms: (a) runoff with high concentration of sediment, (b) flooding in depressions and over a service road. GIS-based simulation of sediment flow rate (a) and overland flow depth (b) using a LiDAR-based DEM and the SIMWE model implemented in GRASS GIS reflects the observed water and sediment flow patterns. Photo courtesy R. McLaughlin, North Carolina State University.

- landscape evolution model *r.landevol* to simulate change in elevation.

The GeoWEPP on-line tool was the easiest to use because the GIS data were provided along with the model interface. The results were limited by resolution of the available data (in this case 30 m) and only annual average soil loss and sediment yield were computed (**Figure 14**). Using the default parameters for central North Carolina, total annual runoff from the watershed was estimated as 2372 m^3 from hillslopes, and sediment yield as 4.9 ton yr^{-1} with erosion rate of 0.5 t (ha yr)$^{-1}$. Deposition was predicted in less than 10% of the area, most likely due to the low resolution of the DEM that did not adequately represent shallow concave landforms.

Annual soil loss and net erosion/deposition was also estimated using the detachment limited and transport capacity limited models combined with the USLE rainfall, soil, and land-cover parameters ($R=220$ and soil erodibility factors ranging between $K=0.15$–0.28 were used). Both models were run in GRASS GIS using map algebra applied to 1 m resolution raster data. The results depicted the spatial pattern of soil detachment (**Figure 15(a)**) and net erosion and deposition (**Figure 15(b)**). The results show significant potential for large rills to develop in the agricultural fields and deposition to occur in the lower section of the valley. Subtle terraces with alternating erosion and deposition in the western, agricultural areas required closer inspection to ensure that they are not artifacts of point cloud measurements or interpolation. The fact that the patterns do not follow the data sampling distribution indicates that the terraces are not data-processing artifacts. The results from terrestrial LiDAR surveys confirm that the subtle terracing is due to the configuration of agricultural fields and direction of tillage.

The detachment capacity limited model (eqn [21]) predicted average annual soil detachment rate of 3.95 t (ha yr)$^{-1}$ for exponent values $m=1.1$ and $n=0.6$. These estimates are in line with the USLE-based Natural Resources Conservation Service (NRCS) erosion rates published for North Carolina, but they are much higher than the values predicted by the GeoWEPP model and those actually measured at the observed values at the watershed outlet. This is due to the fact that the detachment capacity limited models represent soil loss without considering sediment deposition. The estimates from the transport capacity limited model indicate that most of the eroded soil can be deposited within the watershed (i.e., 6.3 ha has a potential for net erosion and deposition will occur over 3.1 ha). The predicted mean deposition rates are higher than mean erosion rates, compensating for the smaller area with potential for deposition. The mean net erosion rate was estimated as 1.4 t (ha yr)$^{-1}$ and mean net deposition rate was 3.9 t (ha yr)$^{-1}$ when $m=1$ and $n=1$ were used. The net soil loss (total erosion minus total deposition) was estimated at 0.48 t (yr^{-1}) assuming vegetation cover, indicating that relatively small amount of sediment will leave the watershed under transport capacity limited conditions.

The SIMWE model was used for single-storm simulations to estimate runoff and sediment transport. The model correctly predicted ponding in the depression created by the road (**Figure 13**). It also provides more realistic pattern of erosion/deposition along the boundaries between the tilled field and

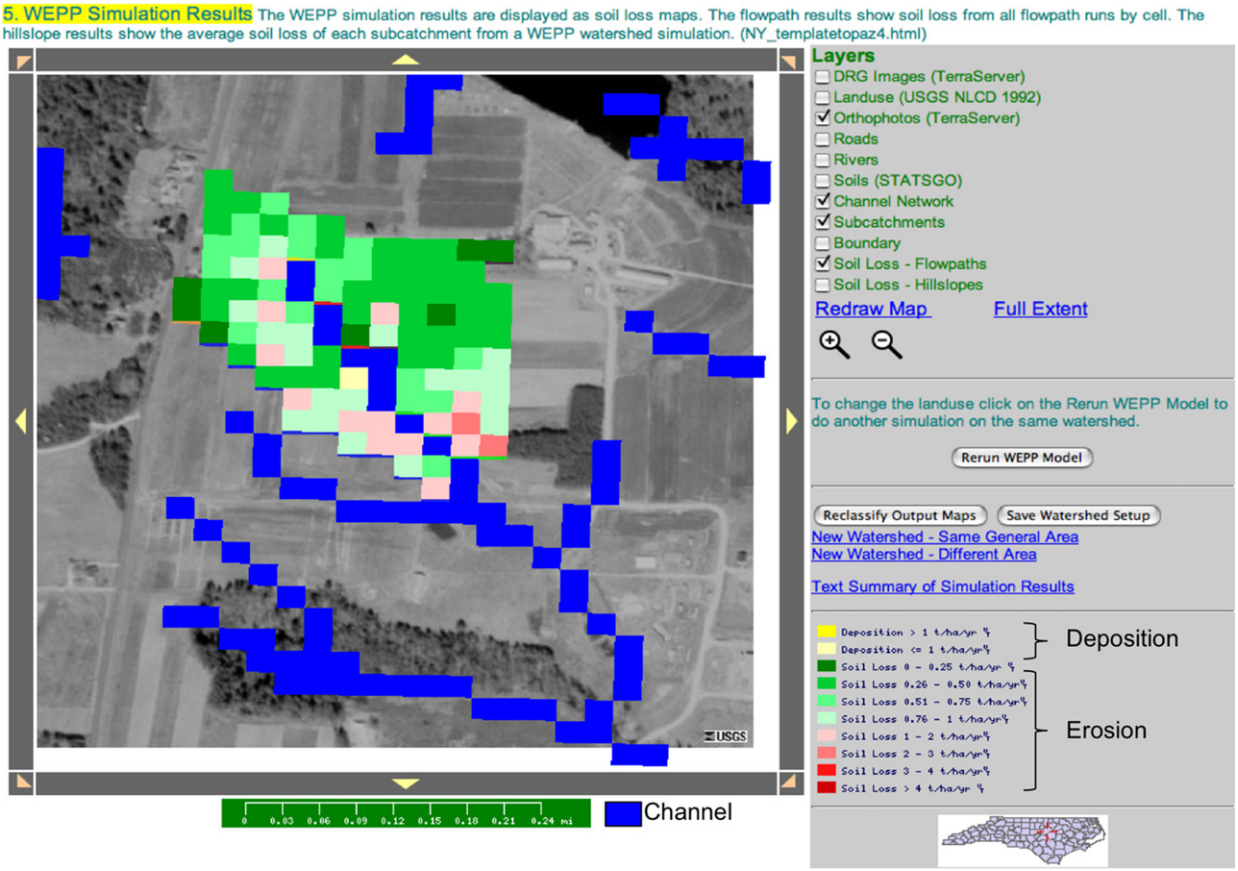

Figure 14 Simulation of hillslope erosion and deposition at 30 m resolution using the Web interface of the GeoWEPP model.

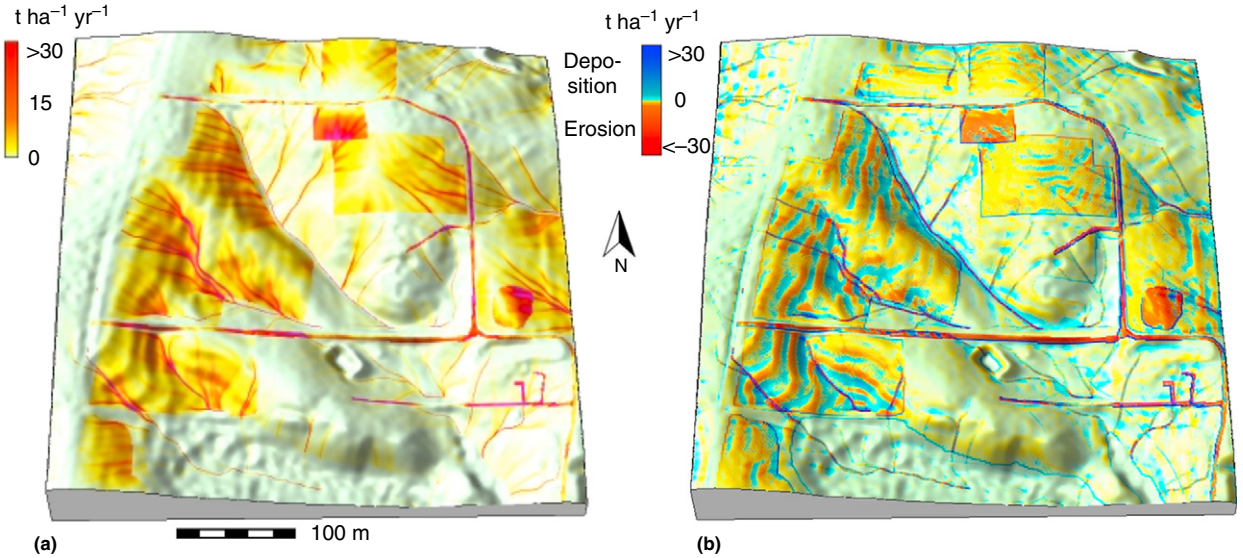

Figure 15 Spatial distribution of (a) soil detachment rate estimated from eqn [21] that includes prediction of high erosion rates due to concentrated water flow; (b) net erosion and deposition rates indicating formation of gullies and subtle terraces predicted from eqn [23]. Higher rates are predicted in areas with crops, dirt roads, and bare soil (see **Figure 12**).

vegetated strip, by allowing gradual deposition over longer flow path, rather than instant deposition, as is the case with the steady-state models. However, the model requires more development and research to support rainfall time-series input, additional channel cross-section geometries, conversion of outputs into commonly used units and measures, and validation with spatially and temporally distributed field data that are only now becoming available from terrestrial laser

scanning technology. It is also computationally much more demanding than the steady-state models.

Although only small changes in elevation are observed during the years with average precipitation, severe storms have occasionally caused major erosion and sediment transport in this area, altering the topography. The landscape evolution model was used to simulate the change in elevation over time due to erosion and deposition by overland flow and diffusive processes between the rainfall events. It was applied to variable land-cover conditions (**Figure 16**) with 40% area in agricultural fields. The results show potential for developing large rills in the fields with subsequent deposition at the edge of the fields and in concave terrain. Under bare ground conditions, the formation of a large gully is predicted along the valley due to concentrated water flow. The simulated erosion and deposition pattern is in general agreement with observations. As in the case of the SIMWE model, repeat terrestrial-laser surveys will provide opportunity to calibrate the model and evaluate its capability to predict the magnitudes and patterns of erosion and deposition.

TanGeoMS was used to explore the impact of various land-design alternatives on surface runoff and soil erosion (**Figure 17**). GIS layers, such as orthophotography, footprints of structures, and flow-accumulation maps were projected over the 1:1200 scale flexible clay terrain model to guide the model modifications. Then various sediment control alternatives were created by modifying the plasticine surface by hand. The modified model was scanned, runoff and erosion were computed in GRASS GIS and resulting animations of water and sediment flow were projected back onto the model to provide rapid feedback on the effects of the proposed change and to guide the next modification (**Figure 17**).

3.9.6.2 Mediterranean Landscape Evolution

The goal of Mediterranean Landscape Dynamics (MedLanD) project was to build a sophisticated modeling laboratory to carry out virtual experiments on the long-term, recursive interactions between society, land-use, and environmental change. Because it aims to simulate high-resolution, real-world landscape dynamics and land-use practices, the MedLanD Modeling Laboratory (MML) is a hybrid modeling environment that tightly couples different modeling approaches (Mayer and Sarjoughian, 2008; Mayer, 2009; Mayer et al., 2006). These include: (1) a GIS-based landscape evolution model that simulates hydrology, erosion/deposition, and vegetation succession; (2) stochastic GIS-based models and dynamic agent-based models (ABM) of farming households and their land-use practices; and (3) regression-based paleoclimate and paleovegetation models (**Figure 18**). Details of the MML are published elsewhere (Barton et al., 2010a, b; Ullah, 2011; Ullah and Bergin, 2011) and only summarized here with emphasis on the landscape evolution modeling component.

In the MML, agropastoral land-use can be modeled stochastically in a GIS or as rule-based actions of independent

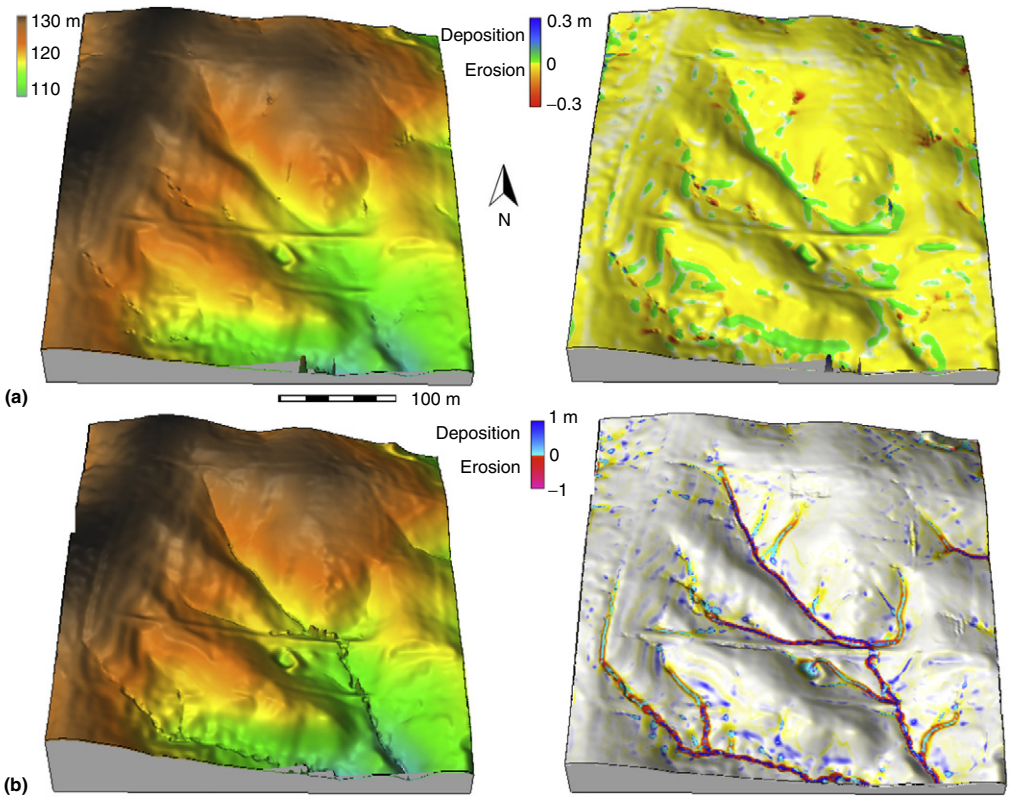

Figure 16 Landscape evolution under different conditions: (a) during small rainfall events erosion rates are low and the valley is filling with deposits, (b) during high intensity rainfall gullies form in locations with concentrated flow. Perspective views of resulting DEMs with elevation color maps are on the left, erosion/deposition pattern is on the right.

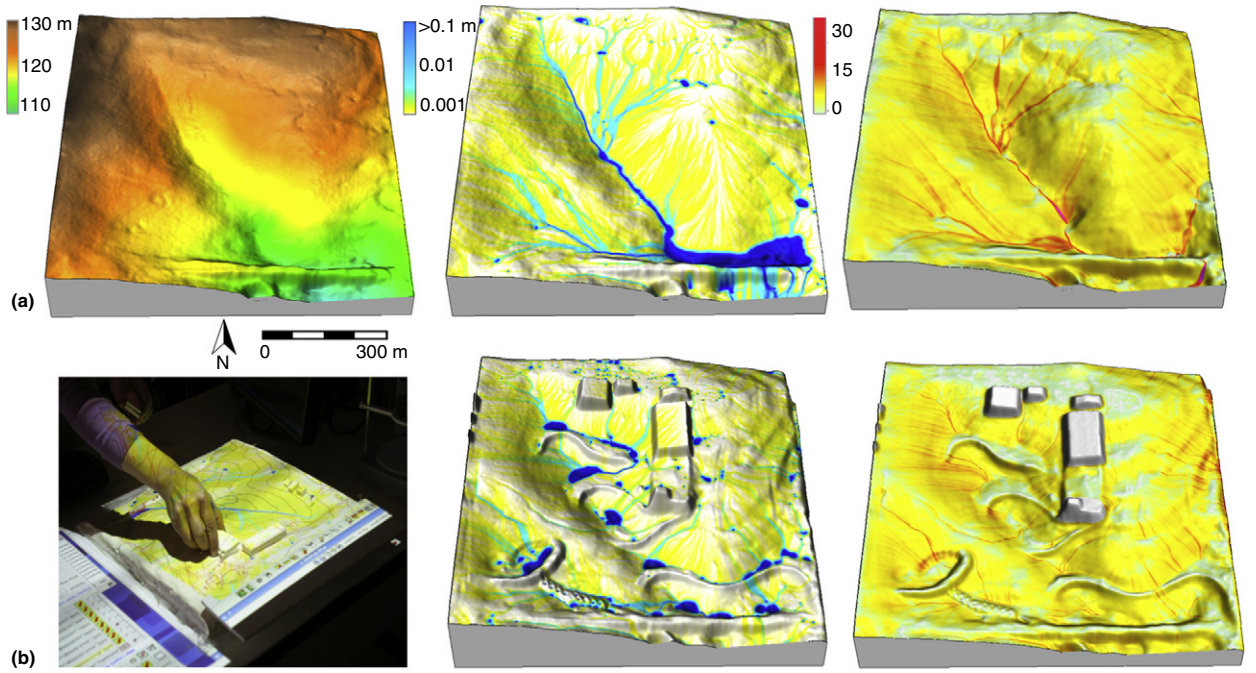

Figure 17 Exploring terrain modification impact on water flow and sediment transport: (a) DEM, water flow depth and topographic erosion potential for the initial model, (b) adding buildings and bio-swales to the model, resulting water flow depth, and topographic erosion potential for the modified model. Model design by B. Harmon (Tateosian et al. 2010).

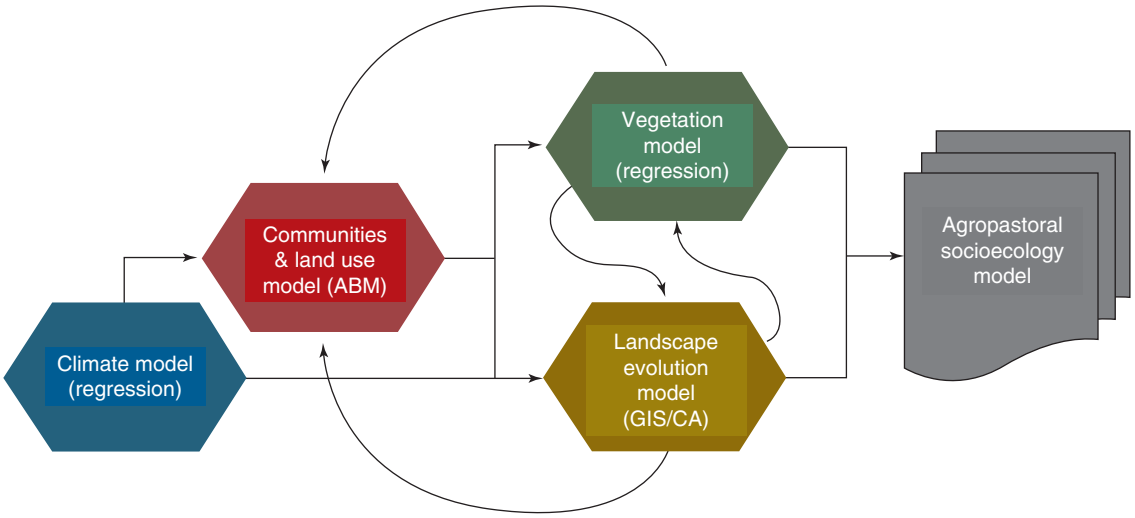

Figure 18 Schematic of the component structure and model couplings for the MedLand Modeling Laboratory.

computer agents in an ABM platform. When modeled stochastically, farming and grazing patches are randomly distributed within catchments, calculated using GIS routines to account for terrain and suitability for farming or herding, around communities (Barton et al., 2010a; Ullah, 2011). Alternatively, individual house-holds can be simulated as virtual agents, organized into villages. Agents choose land to farm or graze on the basis of their need for farming returns (calories that affect birth and death rate), the suitability of land for particular agricultural activities, and costs to use the land, including access on foot and clearance of vegetation (Barton et al., 2010a; Mayer, 2009; Mayer et al., 2006; Ullah and Bergin, 2011). Agents can also collect fuel wood, the amount of which varies according to household size and activities. Whether modeled stochastically or as agent behavior, household land-use can alter the vegetation cover and soil characteristics. These anthropogenic changes to landscapes in turn impact the results of other surface processes on landscapes location and intensity of erosion and deposition. These are simulated in the MML with a landscape evolution model implemented in GRASS GIS as a Python-based script *r.landscape.evol.py* developed by the MedLanD project team.

The model iteratively calculates the amount of erosion and deposition that occurs across the landscape over time. Because each of the process equations described perform better under different topographic conditions, the script uses different process equations for different landforms, and implements them in a manner that optimizes the ratio of model run-time to accuracy of erosion/deposition calculations. The module implements a diffusion equation for areas near drainage divides, a three-dimensional transport capacity limited method for hillslopes and gully heads (eqn [22]), and an equation based on the reach-average shear stress for channels (eqn [10]). It is important to choose the optimal locations on the terrain for the transition between surface process models to ensure that the most appropriate process equation is used for each cell of the DEM. Although these transition points can vary with overall watershed geometry, area, and topographic relief, and also can change during a hydrologic event (e.g., during a storm) as a function of rainfall intensity and duration, they can be estimated in a GIS on the basis of upslope contributing area and topographic profile curvature.

The model employs the advanced flow accumulation and basin analysis module *r.watershed* to calculate upslope contributing area using a multiple flow direction (MFD) algorithm that produces much smoother and more realistic patterns of flow convergence and divergence than does a simpler single flow direction (SFD) D-8 algorithm. Upslope contributing area is then plotted against the profile curvature for each cell (**Figure 19**). Positive values of profile curvature indicate a marked increase in slope (a convex profile), negative values indicate a marked decrease in slope (a concave profile), whereas values close to zero represent cells where there is little change in slope. Drainage divides have little accumulation and little change of slope, plotting near 0 on the x and y axes; hillslopes also have little change in slope, but have higher accumulation, plotting near 0 on the x-axis but higher on the y-axis. The transition between the drainage divide and hillslopes has the maximum convex profile curvature and relatively low values of upslope contributing area, whereas the transition between hillslopes and gully heads at the base of slopes has concave profile curvature and higher contributing area values. Hence, for a given landscape and hydrologic regime, the authors use the value of contributing area for the maximum value of profile curvature for the transition from the diffusion equation to transport capacity limited erosion by overland flow with exponents m, n for sheet wash processes. The value of contributing area the minimum value of profile curvature is used for the transition from sheet wash to transport capacity limited erosion with higher exponents m, n for rill/gully flow (**Figure 19(a)**).

In a similar way, contributing area can be plotted against the tangential curvature of each cell to identify the accumulation value for the transition from the transport capacity limited erosion by overland flow to a shear-stress equation for channelized flow. The beginning of channelized flow can be identified as the location where very low negative values of tangential curvature (concave) are associated with high values of contributing area. Negative values of tangential curvature that are associated with lower values of contributing area represent the larger gullies and gully-heads (i.e., that occur higher in the drainage network than the real stream channels), and even higher values of contributing area where tangential curvature has decreased indicate a widening channel carrying more water (**Figure 19(b)**). **Figure 20** shows the locations of the transition points identified in **Figure 19** on the DEM for which they were derived.

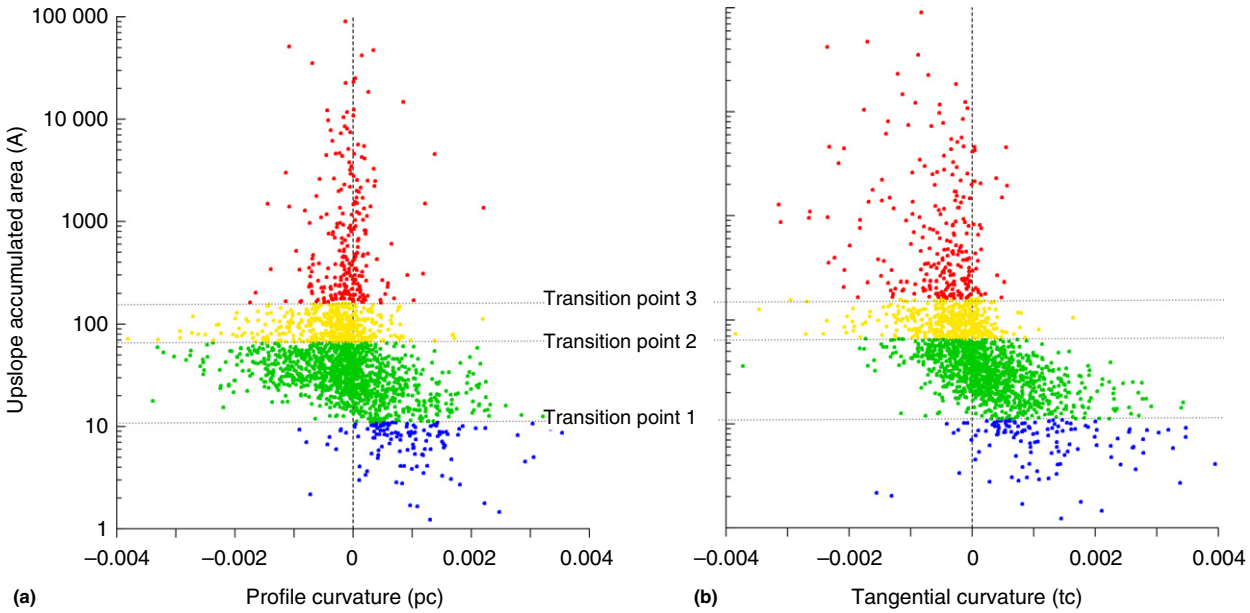

Figure 19 Plot of upslope contributing area vs. profile curvature (pc). Transition point 1 indicates the value of contributing area where the transition from diffusion to sheetwash occurs, and transition point 2 indicates the value of contributing area where transition from sheet wash to rilling/gullying occurs; (b) a plot of contributing area versus tangential curvature (tc). Transition point 3 indicates the value of contributing area where the transition from rilling/gullying to channel flow occurs.

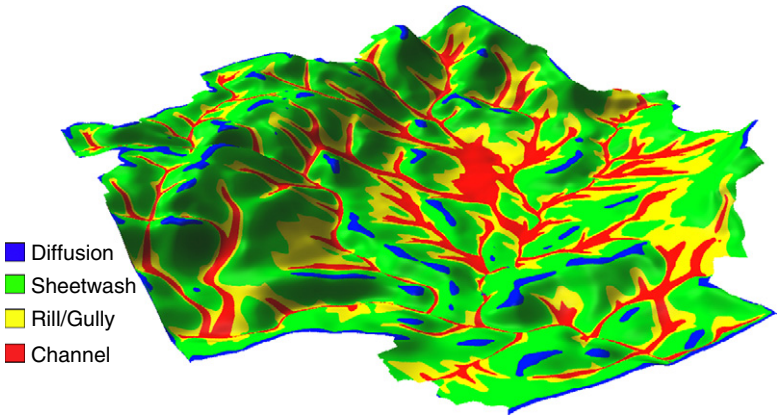

Figure 20 Map showing the location of the process transition points (1, 2, and 3) derived from **Figure 19** draped over a DEM. Actual gullies and channels will be located within the outlined respective areas.

The diffusion equation used by the MML is well-known and simulates soil creep, the movement of soil downslope due to the effect of gravity and particle movement from rainsplash, bioturbation, and other local factors, on portions of the landscape where there is not enough accumulated runoff for overland flow (Tucker and Bradley, 2010):

$$\frac{\partial z}{\partial t} = K_g \nabla^2 z, \qquad [31]$$

where the rate of elevation change is controlled by the diffusion coefficient $K_g(\mathrm{m}(1000\ \mathrm{yr})^{-1})$, for a soil density of 1, which is an empirically derived constant for different climate and vegetation regimes.

The transport capacity limited erosion eqns [22] and [23] used in the MML hillslope model were derived from concepts described by Kirkby (1971), adapted for complex topography by Moore and Burch (1986), and operationalized in GRASS GIS (Mitasova et al., 1996; Mitas and Mitasova, 1998). The approach combines the USLE/RUSLE parameters, slope and upslope contributing area per unit contour width to estimate sediment flow at sediment transport capacity, and calculate net erosion and deposition at the center of each grid cell. Implementation in a GRASS script combines the results of GIS modules for calculating slope, aspect, and flow accumulation using map algebra. Input data for the script include a raster DEM of initial surface topography, soil erodibility (*K*-factor as a constant for uniform soil or a raster map for variable soil), vegetation cover (*C*-factor as a constant or raster map), and rainfall intensity (*R*-factor as a constant only). An underlying bedrock topography DEM is also created to provide a limit the total depth of unconsolidated sediment that can be eroded; when bedrock is reached, soil erodibility is set to near zero. *K*-factor, *C*-factor, and *R*-factor values for RUSLE have been calculated empirically for a variety of settings in the Mediterranean (Boellstorff and Benito, 2005; Essa, 2004; Hammad et al., 2004; Martinez-Casasnovas and Sanchez-Bosch, 2000; Renard et al., 1997; Renard and Freimund, 1994).

For flow in channels, the MML employs a variation of eqn [10], where the shear stress is approximated using eqn [12], but unit stream power eqns [14] and [15] are also considered. In these equations, transport capacity in channels is largely a function of the local slope and the depth of flow. However, depth of flow is difficult to estimate accurately because it is dependent on the local channel geometry and changes over the course of a rainfall event. Therefore, MML estimates flow depth in each cell from an idealized unit hydrograph for that cell using the following equation:

$$h = 2rA/1.25t, \qquad [32]$$

where r (m) is the excess rainfall (precipitation minus infiltration) during a hydrologic event, and $A(\mathrm{m}^2)$ is the upslope contributing area. Then $rA(\mathrm{m}^3)$ is the volume of water that passed over the cell during the simulation interval and t(s) is the number of hydrologic instants in the simulation interval. The hydrologic instant is the time it takes water to cross one cell of a raster DEM, which can be determined by multiplying the average velocity of flowing water in the watershed (e.g., as derived with Manning's eqn [13]) by the cell resolution.

The MML then computes net erosion and deposition rates as divergence in sediment transport capacity (eqn [22]). To approximate the transition between the zones dominated by different processes, sediment flow divergence is computed independently for the zones in which each process is modeled, and the results are then combined into integrated spatial representation of erosion and deposition rates.

For the overland flow driven processes, the net erosion and deposition rates are calculated as units of mass per area per year. To model terrain evolution over time, these rates must be converted to the depth of lost or gained sediment per cell $\Delta z(x, y, t)$ (m) for a given time period Δt based on soil density (eqn [29]). Soil density is approximated using the method outlined by Rawls (1983) combining the percentages of sand, silt, clay, and organic matter, and estimated for Terra Rossa soils (i.e., for Mediterranean landscapes) on the basis of empirical studies by Onori et al. (2006). Similarly as in the gully modeling, the estimated change in elevation is then added to (for deposition) or subtracted from (for erosion) the initial DEM_0, to create a new DEM_1 after a cycle of land-use and terrain change. This process can be iterated repeatedly to simulate decades to millennia of landscape evolution. In addition to the terrain evolution component, other aspects of

the MML simulate vegetation regrowth and recovery of soil fertility for fallowed patches of the landscape. Together, these provide feedbacks to the land-use ABM, affecting subsequent decisions by households about which land to farm and graze.

Initial results using the MML to study the dynamics of ancient land-use and terrain evolution have been promising. In one set of modeling experiments, the MML was parameterized with values derived from ancient farming communities of northern Jordan (**Figure 21**) and used for experiments on the consequences of varying land-use (intensive vs. shifting cereal cultivation, and ovicaprine grazing vs. no grazing) and community size on soil loss and vegetation over the course of two and ten generations, 40 and 200 years respectively (Barton et al., 2010a, b). Some of the modeling results confirm widely held expectations about such land-use: shifting cultivation can cause greater soil loss than intensive, repeated cultivation of a few plots (e.g., with manuring); extensive ovicaprine grazing will cause more erosion than farming without associated grazing; larger communities with more people farming and grazing more land will have a greater impact on the landscape than smaller communities (**Figure 22**). Other results were less intuitively obvious because of the complex interactions between land-use and landscape dynamics. Notably, when community size is below a threshold (whose value is determined by local environmental conditions) the amount of soil loss can be substantially offset by soil accumulation (i.e., by the redeposition of sediments eroded from other parts of a catchment), so that the economic impacts of mixed agropastoral land-use can be negligible or even beneficial. However, if communities pass this threshold size, the consequences change qualitatively such that soil loss greatly exceeds soil accumulation within a land-use catchment. This imbalance continues over the long-term, with the potential for leaving a catchment unsuitable for farming. One mitigating strategy is, not surprisingly, to reduce community size through emigration or fissioning. Another

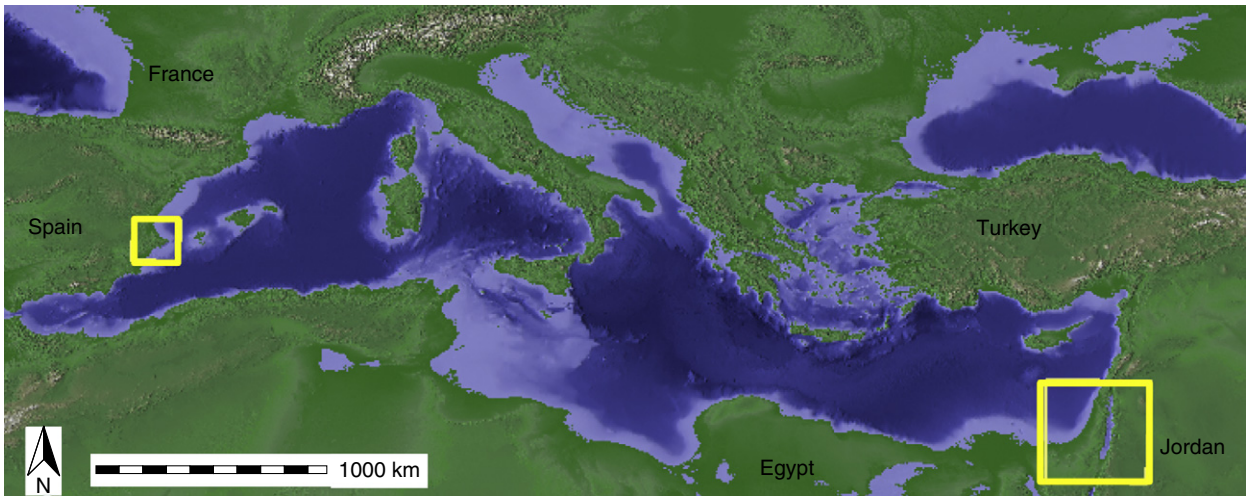

Figure 21 Location of Mediterranean landscapes used in this case study.

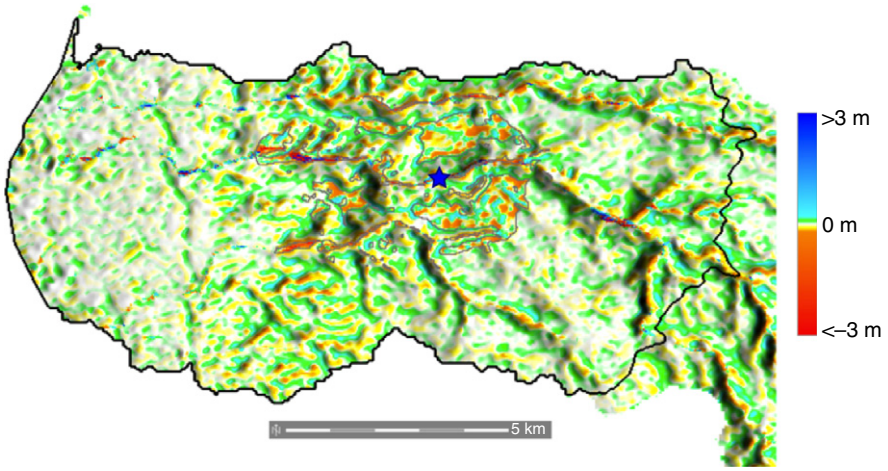

Figure 22 Forty years of cumulative hillslope erosion/deposition around modeled prehistoric farming village (location marked by blue star) in the Wadi Ziqlab drainage of northern Jordan. Dark line marks maximum extent of ovicaprine grazing catchment; grey line marks maximum extent of zone of shifting cultivation around village.

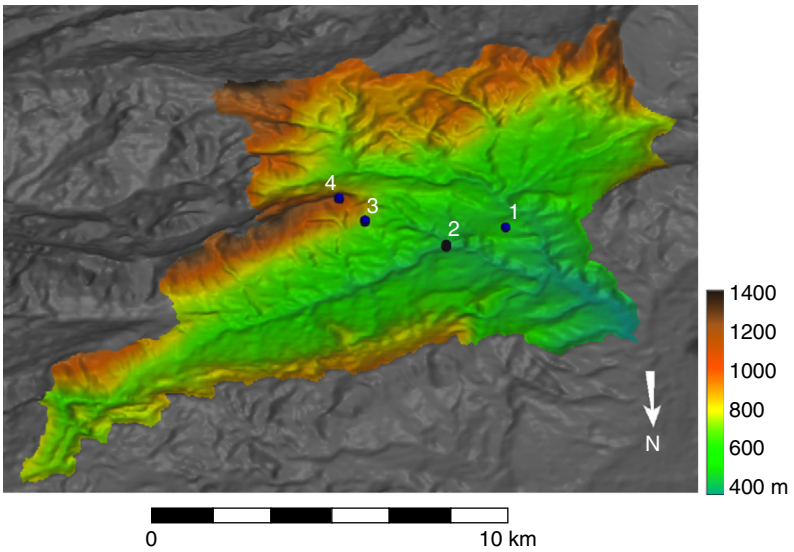

Figure 23 Map of the Rio Penaguila and Rio Serpis valleys showing the different locations and topographic settings of village for each set of experiments: (1) in an alluvial plain (for easy access to land for farming and grazing), (2) in a canyon bottom (for seclusion), (3) at the base of a cliff (for defensibility), and (4) on a topographic prominence (for maximum visibility).

less obvious solution discovered in these experiments is to increase the area devoted to grazing relative to cultivation, moving zones of soil loss into uncultivated uplands and providing more sediment for redeposition in the areas around farmed fields. Conservation measures, like terracing, could also be instituted but would require some degree of social reorganization to ensure the availability of sufficient labor for terrace construction and long-term maintenance. This kind of investment in landesque capital and intensification of land use has often been accompanied by the growth of inequalities in social power and prestige. Comparison with the known archaeological record of this region indicates good agreement between modeling results and both the long-term impacts of Neolithic farming and the social responses to these impacts (Kuijt and Goring-Morris, 2002; Legge and Harris, 1996; Martin, 1999; Quintero et al., 2004; Rollefson and Kohler-Rollefson, 1992; Rosen et al., 2008; Simmons, 2007; Twiss, 2007).

A second set of experiments involved studying the results of situating a small farming village in different topographic contexts in the Rio Penaguila and upper Rio Serpis Valleys of eastern Spain (**Figure 21**), the location of one of the earliest known farming communities in the Iberian Peninsula (Bernabeu et al., 2003; Bernabeu and Kohler, 2005). In four different experimental runs (**Figure 23**): a simulated village, populated by household agents, was set alternatively in an alluvial plain (for easy access to land for farming and grazing); in a canyon bottom (for seclusion); at the base of a cliff (for defensibility); and on a topographic prominence (for maximum visibility).

In each locale, all other initializing parameters besides geographic setting were kept the same for the village. The agents farmed and grazed the land around each site for 100 years and resulting data were collected on population size, economy, vegetation cover, and erosion/deposition (**Figure 24**). When the village was located in the alluvial plain it was more successful initially than when placed in the other settings, as measured in terms of population growth and agricultural returns. However, this success also led to a recursive, self-amplifying growth cycle of increasing population, expanding cultivation and grazing, soil degradation and loss, and even more expansion of cultivation and grazing. When situated in the other locales, the same village grew more slowly and experienced more variable economic returns. However, the smaller and more stable population also had much less detrimental impact on the surrounding landscape (Ullah and Bergin, 2011).

3.9.7 Conclusion and Future Directions

This chapter has presented the underlying theory and methods for GIS-based modeling of soil erosion, sediment transport, and deposition by surface water flow. Although the dynamic models of sediment transport are complex, the topographic controls for most approaches can be approximated using a power function of upslope contributing area and slope. These topographic parameters can be readily extracted from DEMs using GIS tools and they constitute the foundation of GIS-based erosion modeling.

Multitemporal elevation data are becoming available at ever increasing accuracies and at levels of detail that can capture submeter features over large areas, thus providing significant opportunities for improvements in modeling and mapping of soil erosion and deposition. In spite of advances in sensor technologies, spatial representations of soil properties, land cover, and rainfall excess remain weak components of erosion modeling. Uncertainty in these critical input parameters impacts the accuracy of process-based erosion models and the practical solutions require combination of simplified empirical and physics-based models. These models can be calibrated to provide acceptable quantitative summary

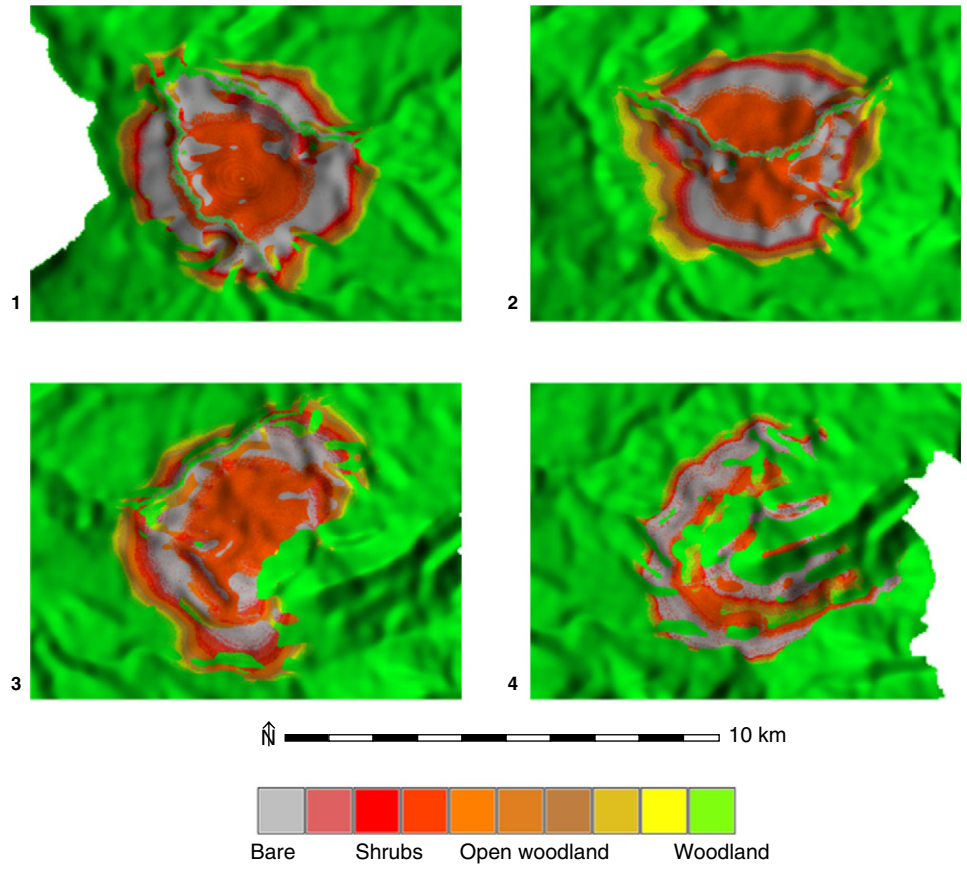

Figure 24 Landcover maps for each modeling experiment with village locations indicated in **Figure 23**.

estimates, such as total volumes or spatially averaged erosion rates, as well as depict the spatial patterns of erosion and deposition. Nevertheless, the accuracy at any point in space and time is often limited. The GIS implementation extends the value and usefulness of these approaches by simulating spatial patterns of erosion and deposition under different existing and future conditions. Such information is critical for erosion and sediment control and invaluable for development of sustainable land-use management practices.

The case studies presented here highlight the use of GIS-based erosion modeling to study the interactions and feedbacks between human activities and erosion processes at different spatial and temporal scales. The first study illustrated the differences in outputs from models at annual and event-based temporal scales. It also introduced an interactive environment - TanGeoMS - for exploration of terrain change impacts on landscape processes with applications for runoff and sediment control design. The second study represents a unique application of erosion and landscape evolution modeling to investigation of relationship between geomorphology and evolution of prehistoric agricultural communities. The simulations highlighted the complexity of feedback mechanisms between the location and size of communities, landforms and their evolution. These examples demonstrate the role of GIS-based erosion modeling in practical problem-solving and in research involving anthropogenic forcing.

Further improvements in the quantitative prediction of sediment transport in space and time may require probabilistic rather than deterministic modeling, as well as a wider use of data assimilation techniques and model ensembles. Spatial analysis and modeling, coupled with advances in laser scanning and hyperspectral technologies provide unique opportunities to address the gaps in our understanding of erosion processes and fundamentally improve both the theory, models, and their GIS implementation.

Acknowledgments

Research results presented in this paper were supported by the US Army Research Office, grant W911NF-04-D-0003-0011, National Science Foundation, grant BCS-410269 North Carolina Water Resources Research Institute. Assistance with data and modeling at the SECREF location by Robert Austin and Richard McLaughlin is greatly appreciated.

References

Arabi, M., Govindaraju, R., Hantush, M., Engel, B., 2006. Role of watershed subdivision on modeling the effectiveness of best management practices with SWAT1. JAWRA Journal of the American Water Resources Association 42(2), 513–528.

Barton, C., Ullah, I., Mitasova, H., 2010a. Computational modeling and neolithic socioecological dynamics: a case study from southwest Asia. American Antiquity 75(2), 364–386.

Barton, C.M., Ullah, I.I., Bergin, S., 2010b. Land use, water and mediterranean landscapes: modeling long-term dynamics of complex socio-ecological systems. Philosophical Transactions of the Royal Society A: Mathematical, Physical and Engineering Sciences 368(1931), 5275–5297.

Bernabeu, J., Kohler, T., 2005. Mas d'Is (Penaguila, alicante): un recinto monumental del VI milenio cal AC. In: Arias, P., Ontanon, R., Garcia- Monco, C. (Eds.), III Congreso sobre el Neolitico en la Peninsula Iberica (Santander, 2003). Instituto Internacional de Investigaciones Prehistoricas de Cantabria, Santander, pp. 485–495.

Bernabeu, J., Kohler, T., Diez, A., Gomez, M., 2003. Mas d'Is (Penaguila, alicante): aldeas y recintos monumentales del neoltico antiguo en el valle del serpis. Trabajos de Prehistoria 60(2), 39–59.

Boellstorff, D., Benito, G., 2005. Impacts of set-aside policy on the risk of soil erosion in central spain. Agriculture, Ecosystems & Environment 107(2–3), 231–243.

Cebecauer, T., Hofierka, J., 2008. The consequences of land-cover changes on soil erosion distribution in Slovakia. Geomorphology 98(3–4), 187–198.

CSMDS, 2011. Community surface dynamics modeling system. 〈http://csdms.colorado.edu/〉.

De Roo, A., Jetten, V., Wesseling, C., Ritsema, C., 1996. LISEM: a physically based hydrological and soil erosion model incorporated in a GIS. IAHS Publication 235, 395–403.

DeRose, R., Gomez, B., Marden, M., Trustrum, N., 1998. Gully erosion in Mangatu Forest, New Zealand, estimated from digital elevation models. Earth Surface Processes and Landforms 23(11), 1045–1053.

Desmet, P., Govers, G., 1995. GIS-based simulation of erosion and deposition patterns in an agricultural landscape: a comparison of model results with soil map information. Catena 25(1–4), 389–401.

Desmet, P., Govers, G., 1996. A GIS procedure for automatically calculating the USLE LS factor on topographically complex landscape units. Journal of Soil and Water Conservation 51(5), 427–433.

Di Luzio, M., Srinivasan, R., Arnold, J., 2002. Integration of watershed tools and SWAT model into BASINS. Journal of the American Water Resources Association 38(4), 1127–1142.

Dingman, S., 2002. Physical Hydrology. Prentice Hall, Upper Saddle River, NJ. vol. 646.

Essa, S., 2004. GIS modeling of land degradation in Northern-Jordan using landsat imagery. In: Proceedings of XXth ISPRS Congress. Istanbul.

Finlayson, D., Montgomery, D., 2003. Modeling large-scale fluvial erosion in geographic information systems. Geomorphology 53(1–2), 147–164.

Flanagan, D., Gilley, J., Franti, T., 2007. Water erosion prediction project(WEPP): development history, model capabilities, and future enhancements. Transactions of the ASAE 50(5), 1603–1612.

Flanagan, D., Nearing, M., 1995. USDA-water erosion prediction project: technical documentation. NSERL Rep 10.

Foster, G., Meyer, L., 1972. A closed form soil erosion equation for upland areas. In: Shen (Ed.), Sedimentation: Symposium to Honor Prof. H.A. Einstein. pp. 12.1–12.19.

Foster, G.R., 1982. Modeling the erosion processes. In: Haan, C.T., Johnson, H.D., Brakensiek, D.L. (Eds.), Hydrologic modeling of small watersheds. ASAE Monograph No. 5, ASAE, St. Joseph, MI, pp. 197–380.

Gaffer, R., Flanagan, D., Denight, M., Engel, B., 2008. Geographical information system erosion assessment at a military training site. Journal of Soil and Water Conservation 63(1), 1.

Govers, G., Giménez, R., Van Oost, K., 2007. Rill erosion: exploring the relationship between experiments, modeling and field observations. Earth- Science Reviews 84(3-4), 87–102.

Govindaraju, R., Kavvas, M., 1991. Modeling the erosion process over steep slopes: approximate analytical solutions. Journal of Hydrology 127(1–4), 279–305.

Haan, C., Barfield, B., Hayes, J., 1994. Design Hydrology and Sedimentology for Small Catchments. Academic Press, New York.

Hammad, A.A., Lundekvam, H., Barresen, T., 2004. Adaptation of RUSLE in the eastern part of the mediterranean region. Environmental Management 34(6), 829–841. http://dx.doi.org/10.1007/s00267-003-0296-7.

Hancock, G., Willgoose, G., Evans, K., 2002. Testing of the SIBERIA land-scape evolution model using the Tin Camp Creek, Northern Territory, Australia, field catchment. Earth Surface Processes and Landforms 27(2), 125–143.

Harmon, R., Doe, W., 2001. Landscape Erosion and Evolution Modeling. Kluwer/ Plenum Publishers, New York.

Hong, S., Mostaghimi, S., 1997. Comparison of 1-D and 2-D modeling of overland runoff and sediment transport. JAWRA Journal of the American Water Resources Association 33(5), 1103–1116.

Jain, M., Das, D., 2010. Estimation of sediment yield and areas of soil erosion and deposition for watershed prioritization using GIS and remote sensing. Water Resources Management 24(10), 2091–2112.

Jetten, V., Govers, G., Hessel, R., 2003. Erosion models: quality of spatial predictions. Hydrological Processes 17(5), 887–900.

Julien, P., Simons, D., 1985. Sediment transport capacity of overland flow. Transactions of the ASAE-American Society of Agricultural Engineers (USA) 28(3), 755–762.

Karssenberg, D., Burrough, P., Sluiter, R., De Jong, K., 2001. The PCRaster software and course materials for teaching numerical modeling in the environmental sciences. Transactions in GIS 5(2), 99–110.

Kheir, R., Wilson, J., Deng, Y., 2007. Use of terrain variables for mapping gully erosion susceptibility in Lebanon. Earth Surface Processes and Land-Forms 32(12), 1770–1782.

Kim, J., Park, Y., Yoo, D., et al., 2009. Development of a SWAT patch for better estimation of sediment yield in steep sloping watersheds1. JAWRA Journal of the American Water Resources Association 45(4), 963–972.

Kirkby, M.J., 1971. Hillslope process-response models based on the continuity equation. Institute of British Geographers Special Pub 3, 15–30.

Koco, Š. 2009. The simulation of gully erosion by geographic information system. Ph.D. thesis, University of Presov, Department of Geography and Regional Development.

Kuijt, I., Goring-Morris, N., 2002. Foraging, farming, and social complexity in the Pre-Pottery neolithic of the southern levant: a review and synthesis. Journal of World Prehistory 16(4), 361–440.

Legge, T., Harris, D., 1996. The beginnings of caprine domestication in south-west asia. The Origins and Spread of Agriculture and Pastoralism in Eurasia. UCL Press, London, pp. 238–262.

Lim, K., Sagong, M., Engel, B., Tang, Z., Choi, J., Kim, K., 2005. GIS-based sediment assessment tool. Catena 64(1), 61–80.

Luo, W., 2001. LANDSAP: a coupled surface and subsurface cellular automata model for landform simulation. Computers and Geosciences 27, 363–367.

Luo, W., Duffin, K., Peronja, E., Stravers, J., Henryb, G., 2004. A web-based interactive landform simulation. Computers & Geosciences 30, 215–220.

Martin, L., 1999. Mammal remains from the eastern jordanian neolithic, and the nature of caprine herding in the steppe. Palorient 25(2), 87–104.

Martínez-Casasnovas, J., Ramos, M., Poesen, J., 2004. Assessment of sidewall erosion in large gullies using multi-temporal DEMs and logistic regression analysis. Geomorphology 58(1–4), 305–321.

Martinez-Casasnovas, J.A., Sanchez-Bosch, I., 2000. Impact assessment of changes in land use/conservation practices on soil erosion in the Peneds-Anoia vineyard region (NE spain). Soil and Tillage Research 57(1–2), 101–106.

Mayer, G.R., Jun. 2009. Composing hybrid discrete event system and cellular automata models. Ph.D. dissertation, Arizona State University.

Mayer, G.R., Sarjoughian, H.S., 2008. A composable discrete-time cellular automaton formalism. First International Workshop on Social Computing, Behavioral Modeling, and Prediction. Springer, Phoenix, AZ, pp. 187–196.

Mayer, G.R., Sarjoughian, H.S., Allen, E.K., Falconer, S.E., Barton, C.M., 2006. Simulation modeling for human community and agricultural landuse. In: Agent-Directed Simulation, Proceedings of the Agent-Directed Simulation Multi-Conference, Huntsville, Alabama. Huntsville, AL, pp. 65–72, April 2–4, 2006.

McLaughlin, R.A., Hunt, W.F., Rajbhandari, N., Ferrante, D.S., Sheffield, R.E., 2001. The sediment and erosion control research and education facility at NC State University. In: Ascough, II J.C., Flanagan, D.C. (Eds.), Soil Erosion Research for the 21st Century. Am. Soc. Ag. Eng., St. Josepth, MI, 2001.

Mitas, L., Brown, W., Mitasova, H., 1997. Role of dynamic cartography in simulations of landscape processes based on multi-variate fields. Computers and Geoscience 23, 437–446.

Mitas, L., Mitasova, H., 1998. Distributed soil erosion simulation for effective erosion prevention. Water Resources Research 34(3), 505–516.

Mitasova, H., Hofierka, J., Zlocha, M., Iverson, L., 1996. Modeling topographic potential for erosion and deposition using GIS. International Journal of Geographical Information Science 10(5), 629–641.

Mitasova, H., Mitas, L., 2002. Modeling physical systems. In: Clarke, K.C., Parks, B.O., Crane, M.P. (Eds.), Geographic Information Systems and Environmental Modeling. Prentice Hall, pp. 189–210.

Mitasova, H., Mitas, L., Brown, W., Johnston, D., 1999. Terrain modeling and soil erosion simulations for Fort Hood and Fort Polk test areas. Research report, University of Illinois, Urbana-Champaign, IL.

Mitasova, H., Mitas, L., Harmon, R., 2005a. Simultaneous spline interpolation and topographic analysis for LiDAR elevation data: methods for open source GIS. IEEE GRSL 2(4), 375–379.

Mitasova, H., Mitas, L., Ratti, C., Ishii, H., Alonso, J., Harmon, R., 2006. Real-time landscape model interaction using a tangible geospatial modeling environment. IEEE Computer Graphics and Applications 26(4), 55–63.

Mitasova, H., Thaxton, C., Hofierka, J., McLaughlin, R., Moore, A., Mitas, L., 2005b. Path sampling method for modeling overland water flow, sediment transport, and short term terrain evolution in Open Source GIS. In: Miller, C., Farthing, M., Gray, V., Pinder, G. (Eds.), Proceedings, XVth International Conference on Computational Methods in Water Resources (CMWR XV). Elsevier, pp. 1479–1490.

Mitchell, J., Engel, B., Srinivasan, R., Wang, S., 1993. Validation of AGNPS for small watersheds using an integrated AGNPS/GIS system. JAWRA Journal of the American Water Resources Association 29(5), 833–842.

Moore, A., McLaughlin, R., Mitasova, H., Line, D., 2007. Calibrating wepp model parameters for erosion prediction on construction sites. Transactions of the ASABE 50(2), 507–516.

Moore, I., Burch, G., 1986. Modeling erosion and deposition: topographic effects. Transactions ASAE 29, 1624–1640.

Moore, I., Wilson, J., 1992. Length-slope factors for the revised universal soil loss equation: simplified method of estimation. Journal of Soil and Water Conservation 47, 423–428.

Morgan, R., Quinton, J., Smith, R., et al., 1998. The European Soil Erosion Model (EUROSEM): a dynamic approach for predicting sediment transport from fields and small catchments. Earth Surface Processes and Landforms 23(6), 527–544.

Murray, A., Paola, C., 1994. A cellular model of braided rivers. Nature 371, 54–57.

Nearing, M., Norton, L., Bulgakov, D., Larionov, G., West, L., Dontsova, K., 1997. Hydraulics and erosion in eroding rills. Water Resources Research 33(4), 865–876.

Nearing, M., Simanton, J., Norton, L., Bulygin, S., Stone, J., 1999. Soil erosion by surface water flow on a stony, semiarid hillslope. Earth Surface Processes and Landforms 24(8), 677–686.

Neteler, M., Mitasova, H., 2008. Open Source GIS: A GRASS GIS Approach. Springer Verlag, New York.

Onori, F., De Bonis, P., Grauso, S., 2006. Soil erosion prediction at the basin scale using the revised universal soil loss equation (RUSLE) in a catchment of Sicily (southern Italy). Environmental Geology 50(8), 1129–1140.

Pandey, A., Chowdary, V., Mal, B., 2009a. Sediment yield modeling of an agricultural watershed using MUSLE, remote sensing and GIS. Paddy and Water Environment 7(2), 105–113.

Pandey, A., Mathur, A., Mishra, S., Mal, B., 2009b. Soil erosion modeling of a Himalayan watershed using RS and GIS. Environmental Earth Sciences 59(2), 399–410.

Park, Y., Kim, J., Engel, B., et al., 2009. Development of web-based SWAT System. Proceedings of ASABE, Reno, Nevada, June 2009.

Peeters, I., Rommens, T., Verstraeten, G., Govers, G., Van Rompaey, A., Poesen, J., Van Oost, K., 2006. Reconstructing ancient topography through erosion modeling. Geomorphology 78(3–4), 250–264.

Pelletier, J., Mitasova, H., Harmon, R., Overton, M., 2009. The effects of interdune vegetation changes on eolian dune field evolution: a numerical-modeling case study at Jockey's Ridge, North Carolina, USA. Earth Surface Processes and Landforms 34(9), 1245–1254.

Pike, A., Mueller, T., Schorgendorfer, A., Shearer, S., Karathanasis, A., 2009. Erosion index derived from terrain attributes using logistic regression and neural networks. Agronomy Journal 101(5), 1068–1079.

Poeter, E., Hill, M., Banta, E., Mehl, S., Christensen, S., 2005. UCODE 2005 and six other computer codes for Universal Sensitivity Analysis, calibration, and uncertainty evaluation, technical report, USGS.

Polyakov, V., Nearing, M., Shipitalo, M., 2004. Tracking sediment redistribution in a small watershed: implications for agro-landscape evolution. Earth Surface Processes and Landforms 29(10), 1275–1291.

Quintero, L.A., Wilke, P.J., Rollefson, G.O., Bienert, H., Gebel, H.G., Neef, R., 2004. Highland towns and desert settlements: origins of nomadic pastoralism in the jordanian neolithic. Central Settlements in Neolithic Jordan. ex oriente, Berlin, pp. 201–213.

Rawls, W.J., 1983. Estimating soil bulk denisty from particle size analysis and organic matter content. Soil Science 135(2), 123.

Renard, K., Foster, G., Yoder, D., McCool, D., 1994. RUSLE revisited: status, questions, answers, and the future. Journal of Soil and Water Conservation 49(3), 213.

Renard, K.G., Foster, G.R., Weesies, G.A., McCool, D.K., Yoder, D.C., 1997. Predicting soil erosion by water: a guide to conservation planning with the revised universal soil loss equation (RUSLE). Agriculture Handbook. US Department of Agriculture, Washington, DC, vol. 703, p. 1251.

Renard, K.G., Freimund, J.R., 1994. Using monthly precipitation data to estimate the r-factor in the revised USLE. Journal of Hydrology 157(1–4), 287–306.

Renschler, C., 2003. Designing geo-spatial interfaces to scale process models: the GeoWEPP approach. Hydrological Processes 17(5), 1005–1017.

Rewerts, C., Engel, B., 1991. ANSWERS on GRASS: integrating a watershed simulation with a GIS. ASAE paper, pp. 91–2621.

Rollefson, G.O., Kohler-Rollefson, I., 1992. Early neolithic exploitation patterns in the levant: cultural impact on the environment. Population and Environment 13, 243–254, NSF Biocomplexity 2002.

Rosen, S.A., Barnard, H., Wendrich, W., 2008. Desert pastoral nomadism in the longue dure: a case study from the negev and the southern levantine deserts. The Archaeology of Mobility: Old World and New World Nomadism. Cotsen Institute of Archaeology. University Of California, Los Angeles, pp. 115–140.

Sheikh, V., van Loon, E., Hessel, R., Jetten, V., 2010. Sensitivity of LISEM predicted catchment discharge to initial soil moisture content of soil profile. Journal of Hydrology 393(3–4), 174–185.

Simmons, A.H., 2007. The Neolithic Revolution in the Near East: Transforming the Human Landscape. University of Arizona Press, Tucson.

Šúri, M., Cebecauer, T., Hofierka, J., Fulajtár, E, 2002. Erosion assessment of Slovakia at a regional scale using GIS. Ecology (Bratislava) 21(4), 404–422.

Tateosian, L., Mitasova, H., Harmon, B., Fogleman, B., Weaver, K., Harmon, R., 2010. TanGeoMS: tangible geospatial modeling system. Visualization and Computer Graphics, IEEE Transactions on 16(6), 1605–1612.

Tucker, G., Bradley, D., 2010. Trouble with diffusion: reassessing hillslope erosion laws with a particle-based model. Journal of Geophysical Research 115, F00A10.

Tucker, G., Lancaster, S., Gasparini, N., Bras, R., 2001a. The channel-hillslope integrated landscape development model (CHILD). In: Harmon, R.S., Doe, W.W. (Eds.), Landscape Erosion and Evolution Modeling. Kluwer/Plenum Publishers, New York, pp. 349–388.

Tucker, G., Lancaster, S., Gasparini, N., Bras, R., Rybarczyk, S., 2001b. An object-oriented framework for distributed hydrologic and geomorphic modeling using triangulated irregular networks. Computers & Geosciences 27(8), 959–973.

Twiss, K.C., 2007. The neolithic of the southern levant. Evolutionary Anthropology 1, 24–35.

Ullah, I., 2011. A GIS method for assessing the zone of human-environmental impact around archaeological sites: a test case from the late neolithic of wadi ziqab, jordan. Journal of Archaeological Science 38(3), 623–632.

Ullah, I.I., Bergin, S., 2011. Modeling the consequences of village site location: least cost path modeling in a coupled GIS and Agent-Based model of village agropastoralism in eastern spain. In: White, D.A., Surface-Evans, S.L. (Eds.), Least Cost Analysis of Social Landscapes: Archaeological Case Studies for Beginners and Experts Alike. University of Utah Press, Salt Lake City.

Van Oost, K., Govers, G., Cerdan, O., et al., 2005. Spatially distributed data for erosion model calibration and validation: The Ganspoel and Kinderveld datasets. Catena 61(2–3), 105–121.

Wainwright, J., Parsons, A., Muller, E., Brazier, R., Powell, D., Fenti, B., 2008. A transport-distance approach to scaling erosion rates: 3. Evaluating scaling characteristics of Mahleran. Earth Surface Processes and Land-forms 33(7), 1113–1128.

Warren, S., Mitasova, H., Hohmann, M., Landsberger, S., Iskander, F., Ruzy-cki, T., Senseman, G., 2005. Validation of a 3-D enhancement of the Universal Soil Loss Equation for prediction of soil erosion and sediment deposition. Catena 64(2–3), 281–296.

Wesseling, C.G., Karssenberg, D., Van Deursen, W.P.A., Burrough, P.A., 1996. Integrating dynamic environmental models in GIS: the development of a dynamic modelling language. Transactions in GIS 1, 40–48.

Willgoose, G., 2004. Mathematical modeling of whole landscape evolution. Annual Review of Earth and Planetary Sciences 33(1), 443.

Willgoose, G., Bras, R., Rodriguez-Iturbe, I., 1991. A coupled channel network growth and hillslope evolution model: 2. Nondimensionalization and applications. Water Resources Research 27(7), 1685–1696.

Wischmeier, W., Smith, D., 1978. Predicting Rainfall Erosion Losses: A Guide to Conservation Planning United States. Dept. of Agriculture. Agriculture Handbook, Washington, DC.

Woodward, D., 1999. Method to predict cropland ephemeral gully erosion. Catena 37(3–4), 393–399.

Biographical Sketch

Helena Mitasova is an Associate Professor at the Department of Marine, Earth, and Atmospheric Sciences, North Carolina State University in Raleigh, NC, USA. She co-authored the first book on open source GRASS GIS and published more than 50 papers on methods and applications of topographič analysis, erosion modeling, coastal dynamics, and visualization. Her PhD is from the Slovak Technical University, Bratislava, Slovakia.

C. Michael Barton is a Director of the Center for Social Dynamics and Complexity and a Professor of Anthropology in the School of Human Evolution and Social Change at Arizona State University. Barton's research interests center around long-term human ecology and the dynamics of Quaternary landscapes. He heads an international, multidisciplinary team studying the long-term socioecology of the beginnings of agriculture. He also is active in the development and application of spatial technologies in archaeology and serving on the open source GRASS GIS development team. He holds a PhD from the University of Arizona in anthropology and geosciences.

Isaac Ullah is a PhD candidate in the School of Human Evolution and Social Change at Arizona State University, Tempe, USA. He is a member of the Mediterranean Land-scape Dynamics project, and specializes in geological applications in archaeology using GIS and modeling techniques. He studies the long term effects of human land use decisions and how potential anthropogenic environmental degradation may have affected settlement patterns. He holds an MA in Anthropology from the University of Toronto.

Jaroslav Hofierka is an Associate Professor at the Institute of Geography, Faculty of Sciences, Pavol Jozef Safarik University, Kosice, Slovakia. His research activities include digital terrain modeling, geomorphometry, erosion risk analysis as well as solar radiation and 3D city modeling. He has been active in open source GIS development and has contributed several core modules to GRASS GIS. He received a PhD degree in Cartography and GIScience from the Comenius University, Bratislava, Slovakia.

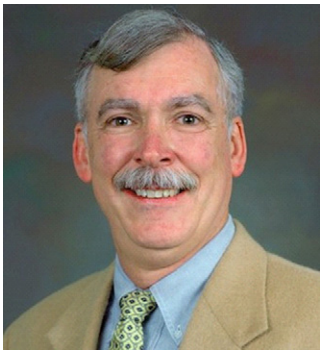

Russell S. Harmon is an Adjunct Associate Professor at North Carolina State University and he has been a Program Manager at the Army Research Office, where he is responsible for the ARO extramural basic research program in terrestrial sciences. He is a Fellow of the Army Research Laboratory, Geological Society of America, and National Speleological Society and is current Past-President of the International Association of GeoChemistry. Dr. Harmon is actively engaged in research in landscape dynamics and geospatial analysis, riverine geo-chemistry, and laser-induced breakdown spectroscopy. He holds a MS from the Pennsylvania State University, and PhD from the McMaster University.